

000 001 002 003 004 005 006 007 008 009 010 011 012 013 014 015 016 017 018 019 020 021 022 023 024 025 026 027 028 029 030 031 032 033 034 035 036 037 038 039 040 041 042 043 044 045 046 047 048 049 050 051 052 053 TOWARD FINE-GRAINED DOMAIN KNOWLEDGE: CURRICULUM PSEUDO-LABELING FOR ONLINE TEST-TIME ADAPTATION

006 **Anonymous authors**

007 Paper under double-blind review

011 ABSTRACT

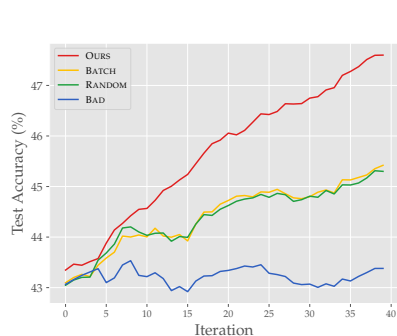
013 Online Test-Time Adaptation (OTTA) aims to adapt a pre-trained model to unlabeled test instances under domain shift in an online manner, where domain knowledge that the model accumulates from previously observed mini-batches directly affects its predictions on subsequent instances. Most previous OTTA methods exploit domain knowledge at a coarse-grained batch level, which prevents the model from fully absorbing the domain knowledge. To deal with this problem, we propose a novel framework CUrriculum Pseudo-Labeling for Online Test-time adaptation (CUPLOT), which further mines orderly domain knowledge at a fine-grained instance level. Specifically, CUPLOT prepares the arriving batch as a series of curricula based on the modeled relevance of domain knowledge between the model and instances. Then, the model orderly learns the instances with pseudo-labels generated by class prototypes in each curriculum. In this way, the domain knowledge is accumulated in a fine-grained manner through instances of curricula rather than mini-batches, improving the absorption of domain knowledge and the performance of the model. Theoretically, we prove that the curriculum pseudo-labels could enable the model to have a stronger adaptation ability, resulting in a tighter bound of approaching the Bayes optimal classifier on the target domain.

030 1 INTRODUCTION

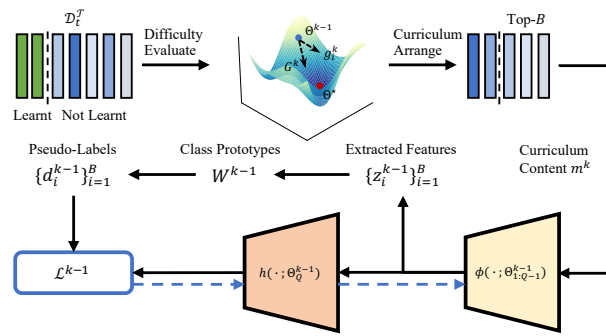
032 Online Test-Time Adaptation (OTTA), an emerging paradigm, aims to continue to train a pre-trained model with unlabeled instances from a different target domain in an online manner during test time. Due to the difficulty in collecting training samples from the source domain exactly identical to the target domain encountered during testing, the need to adapt the model in the test phase leads to various applications for OTTA techniques, such as medical image analysis (He et al., 2021; Ma et al., 2022), autonomous driving (Volpi et al., 2022; Bahmani et al., 2023), and speech processing (Lin et al., 2022; Kim et al., 2022).

039 In OTTA, the model can't access previously observed mini-batches, yet it can accumulate domain knowledge, which directly impacts its predictions on subsequent instances. To accomplish the OTTA task, many approaches have been proposed to exploit domain knowledge in unlabeled test instances. Wang et al. (2020); Gong et al. (2022); Mirza et al. (2022); Zhao et al. (2023) modulate the statistics of the batch normalization layer to update domain knowledge of the model when a test mini-batch arrives. Zhang et al. (2022); Jing et al. (2022); Niu et al. (2023); Lee et al. (2024) perform entropy minimization to satisfy the necessary condition to have learned domain knowledge, i.e., more confident predictions on test instances. Iwasawa & Matsuo (2021); Goyal et al. (2022); Shin et al. (2022); Yang et al. (2022); Döbler et al. (2023); Jang et al. (2023); Wang et al. (2023); Sun et al. (2024) focus on generating pseudo-labels for unlabeled test instances to build an empirical risk estimator, enabling the model to absorb domain knowledge in a supervised learning manner.

050 Intuitively, the more domain knowledge accumulated from each batch, the more beneficial it is for 051 subsequent predictions. However, most previous OTTA methods only exploit domain knowledge at a 052 coarse-grained batch level, limiting the absorption of the domain knowledge from some representative 053 instances. For instance, if the gradient on an instance is more inconsistent with the overall gradient on the batch, its domain knowledge will be diluted or even harm the absorption of domain knowledge



(a) Adaptation accuracy on CIFAR-100-C.



(b) Overview of our approach CUPLOT.

Figure 1: (a) Experimental evidence showing that our gradient-consistency curriculum achieves consistently stronger online adaptation than random, bad, or batch orders on CIFAR-100-C, demonstrating that learning order directly influences the absorption of domain knowledge. (b) Detailed pipeline of the proposed curriculum-driven online adaptation framework at one curriculum.

from other instances, leading to less knowledge being absorbed at the batch level. Empirically, we conduct an additional experiment comparing four learning orders on CIFAR-100-C: (1) our gradient-consistency curriculum order, (2) a random order, (3) an intentionally poor order obtained by reversing the ranked scores, and (4) ordinary batch. As illustrated in Figure 1(a), the adaptation accuracy curves across the test stream show that reasonable ordering consistently achieves higher accuracy than other cases under identical settings, demonstrating that the order in which samples are learned affects how effectively fine-grained domain knowledge is absorbed during online adaptation. Note that without deliberately organizing the learning order of samples, there may even exist learning sequences under which the model almost fails to adapt.

Hence, in this paper, we propose to further mine domain knowledge at a more fine-grained instance level by considering the learning sequence of the instances within each batch from two aspects showed in Figure 1(b). First, the arrived batch is organized as a series of curricula based on the modeled relevance of domain knowledge between what has been learned by the model and what is about to be learned by the model. Second, the model orderly learns the instances with pseudo-labels generated by class prototypes in each curriculum. The proposed framework is named CUPLOT, i.e., *Curriculum Pseudo-Labels for Online Test-time adaptation*, which accumulates the domain knowledge in a more fine-grained manner through instances of curricula rather than mini-batches, improving the absorption of domain knowledge and the performance of the model. **CUPLOT introduces a curriculum mechanism specifically tailored for OTTA by defining easy and hard instances through gradient consistency, a label-free measure reflecting whether a sample's gradient aligns with the dominant update direction.** Our contributions are summarized as follows:

- Practically, we propose a curriculum learning framework for OTTA, which prepares the arriving batch as organized curricula and generates pseudo-labels deeply dependent on the curricula, improving the absorption of domain knowledge at a fine-grained level.
- Theoretically, we demonstrate that the curriculum pseudo-labels could enable the model to have a stronger adaptation ability, resulting in a tighter bound of approaching the Bayes optimal classifier on the target domain.

2 RELATED WORKS

Problem setting. Online Test-Time Adaptation (OTTA), a practical learning process to deal with domain shift (Ben-David et al., 2010; Saenko et al., 2010; Lu et al., 2020), attempts to update parameters of the predictive model already trained on a source domain dataset by processing unlabeled mini-batch datasets from a target domain in a streaming manner with no access to the source domain dataset. Recently, various approaches have been proposed to contribute to OTTA.

Adaptation methods. Batch-normalization-based approaches (Wang et al., 2020; Gong et al., 2022; Mirza et al., 2022; Zhao et al., 2023) adjust the statistics of the batch normalization layer to update

108 the model’s domain knowledge upon the arrival of a test mini-batch. For example, Wang et al. (2020)
 109 suggest updating the batch normalization statistics in the pre-trained model by using the estimated
 110 statistics from the online test batch. Mirza et al. (2022) stabilize the running mean and variance in
 111 batch normalization by augmenting the incoming instance to form a tiny batch and introducing the
 112 decaying momentum for the mean and variance. Gong et al. (2022) and Zhao et al. (2023) further
 113 address class bias through sampling and weighting techniques during estimating normalization
 114 statistics, respectively.

115 Entropy-minimization-based approaches (Zhang et al., 2022; Jing et al., 2022; Niu et al., 2023; Lee
 116 et al., 2024) conduct entropy minimization to learn domain knowledge, since a well-adapted model
 117 outputs more confident predictions on test instances. Zhang et al. (2022) focus on single-instance
 118 robustness and suggest minimizing the entropy calculated from the average output distribution of
 119 the model across various augmentations. Jing et al. (2022) utilize the entropy loss as the likelihood
 120 function and put forward a variational model perturbation approach. Moreover, Niu et al. (2023) and
 121 Lee et al. (2024) select part of the arriving instances to perform reliable entropy minimization.

122 Pseudo-labeling-based approaches (Iwasawa & Matsuo, 2021; Goyal et al., 2022; Shin et al., 2022;
 123 Yang et al., 2022; Döbler et al., 2023; Jang et al., 2023; Wang et al., 2023; Sun et al., 2024)
 124 attempt to generate high-quality pseudo-labels for unlabeled test instances to perform empirical
 125 risk minimization, which allows the model to absorb domain knowledge in a supervised learning
 126 manner. For instance, based on the distances in feature space. Iwasawa & Matsuo (2021) build a
 127 pseudo-prototype for each class, which has the ability to classify new samples. Goyal et al. (2022)
 128 utilize a derived conjugate pseudo label to train the model in a self-training manner. Shin et al.
 129 (2022) combine predictions from multiple modalities to generate pseudo-labels with a selective fusion
 130 strategy. Meanwhile, Yang et al. (2022) average the predictions of neighboring samples stored in a
 131 memory bank to produce soft pseudo-labels. Jang et al. (2023) intend to ensure prediction consistency
 132 between prototype-based and neighbor-based classifiers. Wang et al. (2023) aim at feature alignment
 133 and uniformity through the test-time self-distillation and memorized spatial local clustering. Sun et al.
 134 (2024) refine the generation process of pseudo-labels by integrating the previous prototype-based and
 135 nearest-neighbor methods as a prototype-based graph model.

136 **More recently, a complementary line of work Wang et al. (2022); Döbler et al. (2023); Sójka et al.
 137 (2023), especially the effective approach RMT Döbler et al. (2023), focuses on the setting of Continual
 138 Test-Time Adaptation (CTTA) and adopts teacher-student consistency, which provides highly stable
 139 adaptation in non-stationary environments through teacher–student consistency.**

140 **Connection to Curriculum learning.** Most previous OTTA methods only absorb domain knowledge
 141 at a coarse-grained batch level, limiting the absorption of the domain knowledge. Motivated by
 142 curriculum learning (Bengio et al., 2009; Kumar et al., 2010; Zhou et al., 2020b; Abbe et al., 2023),
 143 where a model is trained from easier instances to harder ones by emulating meaningful learning
 144 sequence in human curricula, we propose the CUPLOT framework. **Compared to previous curriculum
 145 learning work (Zhou et al., 2020a; Zhang et al., 2021; Karim et al., 2023) in related fields, which
 146 primarily focus on the absorption of in-class knowledge, our proposed framework emphasizes on
 147 the systematic acquisition of domain knowledge under shift and is directly grounded in optimization
 148 dynamics and supported by solid theoretical foundations.** Specifically, the adapted model is expected
 149 to first learn the easier instances containing domain knowledge relevant to the already learned domain
 150 knowledge, and then attempt to conquer the harder instances containing deep domain knowledge.

151 3 PROPOSED METHOD

152 3.1 PRELIMINARIES

153 **Online Test-time Adaptation.** Following the literature Yu Sun (2020); Boudiaf et al. (2022); Zhao
 154 et al. (2023); Shuaicheng Niu (2024), we consider the multi-class classification Ian Goodfellow &
 155 Bengio (2016) as the original training task for TTA. Let $\mathcal{X} \subset \mathbb{R}^q$ denote the q -dimensional instance
 156 space, $\mathcal{Y} = \{1, 2, \dots, c\}$ be the label space, where c is the number of classes, $\mathcal{D}_S = \{(\mathbf{x}_i, y_i)\}_{i=1}^{n^0}$
 157 be the dataset from the source domain S , where the instance $\mathbf{x}_i \in \mathcal{X}$ and correct label $y_i \in \mathcal{Y}$ is
 158 independently sampled from a joint distribution $p_S(\mathbf{x}, y)$, $\mathcal{D}_{\mathcal{T}} = (\mathcal{D}_{\mathcal{T}}^1, \mathcal{D}_{\mathcal{T}}^2, \dots, \mathcal{D}_{\mathcal{T}}^T)$ be a sequence
 159 of unlabeled mini-batches from the target domain \mathcal{T} , where $\mathcal{D}_{\mathcal{T}}^t = \{\mathbf{x}_i^t\}_{i=1}^{n^t}$ is the received mini-
 160 batch dataset at the t -th step during test-time inference and the observed instance $\mathbf{x}_i^t \in \mathcal{X}$ with
 161

162 unobserved correct label $y_i^t \in \mathcal{Y}$ is subject to a misaligned joint distribution $p_{\mathcal{T}}(\mathbf{x}, y) \neq p_{\mathcal{S}}(\mathbf{x}, y)$,
 163 $f(\cdot; \Theta) : \mathcal{X} \mapsto \Delta^{c-1}$ denote the predictive model f parameterized by Θ , where Δ^{c-1} is the
 164 c -dimensional probability simplex.

165 In TTA, we have completed the training of the prediction model f on the source domain dataset $\mathcal{D}_{\mathcal{S}}$,
 166 and its parameters have been updated to Θ^0 . Given the received mini-batch dataset $\mathcal{D}_{\mathcal{T}}^t$ at t -th step,
 167 we aims to update the parameters of the predictive model from Θ^{t-1} to Θ^t , such that it could assign
 168 each instance \mathbf{x}_i^t with its correct label y_i^t . Overall, TTA attempts to maximize the following objective:
 169 $\mathcal{O} = \frac{\sum_{t=1}^T \sum_{i=1}^{n^t} \mathbb{I}[y_i^t = \arg \max_{j \in \mathcal{Y}} f_j(\mathbf{x}_i^t; \Theta^t)]}{\sum_{t=1}^T n^t}$, where $\mathbb{I}[\cdot]$ is the indicator function. Note that we follow
 170 the same protocol as (Yu Sun, 2020) where optimization is performed ahead of evaluation.
 171

172 **Curriculum learning.** Curriculum learning improves optimization by presenting training samples
 173 in a deliberately ordered sequence. A curriculum is a permutation $\pi : \{1, \dots, n\} \rightarrow \{1, \dots, n\}$
 174 that determines the learning order $(\mathbf{x}_{\pi(1)}, \dots, \mathbf{x}_{\pi(n)})$. Denote by $\Theta_t(\pi)$ the model parameters after
 175 sequentially observing the first t examples under π . The goal is to identify an optimal ordering π^*
 176 that yields the generalization error after completing training. Intuitively, an effective curriculum first
 177 leverages easy or reliable instances, guiding the optimizer toward a stable region of the parameter
 178 space; subsequent harder or noisier samples are then leveraged to refine the decision boundary.
 179

180 3.2 THE CUPLOT FRAMEWORK

181 Our CUPLOT framework aims to allow the predictive model to learn at the t -th batch with a more
 182 optimal instance sequence, thereby enabling the model to absorb the domain knowledge of the target
 183 domain more effectively. Specifically, the optimization step for the t -th batch is further decomposed
 184 into $K^t \in \{1, 2, \dots, n^t\}$ ordered curricula, each of which uses only a selected subset of the received
 185 batch $\mathcal{D}_{\mathcal{T}}^t$ for the optimization of the predictive model.
 186

187 Let $\mathbf{M}^t = [\mathbf{m}^{t,1}; \mathbf{m}^{t,2}; \dots; \mathbf{m}^{t,K^t}]^\top \in \{0, 1\}^{K^t \times n^t}$ to represent the sequence matrix of curriculum
 188 content, where the vector $\mathbf{m}^{t,k} = [m_1^{t,k}, m_2^{t,k}, \dots, m_{n^t}^{t,k}] \in \{0, 1\}^{n^t}$ indicates whether the instance
 189 $\mathbf{x}_i^t \in \mathcal{D}_{\mathcal{T}}^t$ should be included as the content of the k -th curriculum and participate in the k -th sub-step
 190 optimization. Then, the overall optimization of Θ^{t-1} at the t -th batch is formulated as:
 191

$$\Theta^t = \Theta^{t-1} - \alpha \sum_{i=1}^{n^t} \sum_{k=1}^{K^t} m_i^{t,k} \frac{\partial \ell(f(\mathbf{x}_i^t; \Theta^{t-1, k-1}), \mathbf{d}_i^{t,k})}{\partial \Theta^{t-1, k-1}}, \quad (1)$$

195 with the curriculum content matrix \mathbf{M}^t is subject to

$$\forall 1 \leq k' \leq K^t, \sum_{k=1}^{k'} \sum_{i=1}^{n^t} m_i^{t,k} \leq n^t, \prod_{k=1}^{k'} \mathbf{m}^{t,k} = \mathbf{0}. \quad (2)$$

200 Here, α is the step size of the optimization, ℓ is the cross-entropy loss, and $\mathbf{d}_i^{t,k} =$
 201 $[d_{i,1}^{t,k}, d_{i,2}^{t,k}, \dots, d_{i,c}^{t,k}] \in \mathbb{R}^c$ denotes the curriculum pseudo-label of the instance \mathbf{x}_i^t with $\sum_{j=1}^c d_{i,j}^t = 1$.
 202 Besides, at the k -th curriculum within the t -th batch, the model parameters is updated from $\Theta^{t-1, k-1}$
 203 to $\Theta^{t-1, k}$ in Eq. (1) as follows:
 204

$$\Theta^{t-1, k} = \Theta^{t-1, k-1} - \alpha \sum_{i=1}^{n^t} m_i^{t,k} \frac{\partial \ell(f(\mathbf{x}_i^t; \Theta^{t-1, k-1}), \mathbf{d}_i^{t,k})}{\partial \Theta^{t-1, k-1}}, \quad (3)$$

208 where $\Theta^{t-1, 0} = \Theta^{t-1}$ at the beginning step when $k = 1$.
 209

210 Next, we program the sequence of course content \mathbf{M}^t in Eq. (1) to activate our curriculum framework
 211 by resorting to gradient consistency $\boldsymbol{\mu}^{t,k} = [\mu_1^{t,k}, \mu_2^{t,k}, \dots, \mu_{n^t}^{t,k}] \in \mathbb{R}^{n^t}$ to decide the k -th curriculum
 212 content $\mathbf{m}^{t,k}$. Adopting reverse thinking, if the gradient on an instance is more inconsistent with the
 213 overall gradient on the batch, its knowledge will be diluted and less knowledge will be absorbed by
 214 the model at the batch level. Therefore, during our more fine-grained instance-level learning, such an
 215 instance should be scheduled for later in the learning curriculum. This is in the hope that after the
 model has learned more domain knowledge, it will be able to effectively learn from such an instance.

216 On one hand, the gradient $\mathbf{g}_i^{t,k}$ on the instance \mathbf{x}_i^t is calculated as follows:
 217

$$218 \quad \mathbf{g}_i^{t,k} = \frac{\partial \ell(f(\mathbf{x}_i^t; \Theta^{t-1,k-1}), \mathbf{d}_i^{t,k-1})}{\partial \Theta^{t-1,k-1}}. \quad (4)$$

221 On the other hand, the gradient on the content to be learned $\mathbf{G}^{t,k}$ is calculated as follows:
 222

$$223 \quad \mathbf{G}^{t,k} = \sum_{i=1}^{n^t} (\mathbf{1} - \mathbf{s}_i^{t,k-1}) \frac{\partial \ell(f(\mathbf{x}_i^t; \Theta^{t-1,k-1}), \mathbf{d}_i^{t,k-1})}{\partial \Theta^{t-1,k-1}}, \quad (5)$$

226 where the vector $\mathbf{s}^{t,k-1} = [s_1^{t,k-1}, s_2^{t,k-1}, \dots, s_{n^t}^{t,k-1}] \in \{0, 1\}^{n^t}$ denotes the cumulative curriculum
 227 content consisting of the learned instances before the k -th step within t -th batch, i.e., $\mathbf{s}^{t,k-1} =$
 228 $\sum_{k'=1}^{k-1} \mathbf{m}^{t,k'}$ if $k-1 \geq 1$, and thus $\mathbf{1} - \mathbf{s}_i^{t,k-1}$ denotes the content to be learned. When $k=1$, we
 229 set $\mathbf{s}^{t,k-1} = \mathbf{0}$ and $\mathbf{d}_i^{t,k-1} = f(\mathbf{x}_i^t; \Theta^{t-1,k-1})$.
 230

231 Based on Eq. (4) and (5), the gradient consistency $\mu_i^{t,k}$ for the instance \mathbf{x}_i^t is measured as follows:
 232

$$233 \quad \mu_i^{t,k} = \frac{1}{\|\mathbf{G}^{t,k} - \mathbf{g}_i^{t,k}\|_1}, \quad (6)$$

235 whose larger value indicates that the gradients are more consistent. In practice, when $k-1$ curriculum
 236 steps have selected samples, the remaining samples in the k -th step are simply all the unselected
 237 samples, and no further selection is needed.
 238

After obtaining the gradient consistency $\mu^{t,k}$, we generate the k -th curriculum content:
 239

$$240 \quad \mathbf{m}^{t,k} = (\mathbf{1} - \mathbf{s}^{t,k-1}) \cdot \psi(\mu^{t,k}), \quad (7)$$

241 where $\psi : \mathbb{R}^{n^t} \mapsto \{0, 1\}^{n^t}$ with $\psi_i(\mu^{t,k}) = \mathbb{I}[\mu_i^{t,k} \geq \delta]$, and δ is a threshold employed to sieve
 242 the instance according to the gradient consistency $\mu^{t,k}$. Practically, by considering efficiency while
 243 adapting, the threshold δ is usually set as the top- B value of the vector $\mu^{t,k} \cdot (\mathbf{1} - \mathbf{s}^{t,k-1})$ with
 244 $B = \text{round}(\log(1 - \mathbf{s}^{t,k-1}))$, and the number of scheduled curricula K^t is set around $\log n^t$. B is
 245 chosen so that after K^t curriculum steps, all samples in the batch are covered, ensuring a complete
 246 and well-structured curriculum.
 247

Then, we consider the generation of the pseudo label $\mathbf{d}_i^{t,k}$ in Eq. (1) and (3). The pseudo-label
 248 $\mathbf{d}_i^{t,k}$ deeply depends on the previously learned curriculum content, and thus is called curriculum
 249 pseudo-labeling in our framework. Specifically, if $m_i^{t,k} = 1$, the curriculum pseudo-label \mathbf{d}_i^t of the
 250 instance \mathbf{x}_i^t will be generated as follows:
 251

$$252 \quad \mathbf{d}_i^{t,k} = \text{Softmax}(\mathbf{z}_i^{t,k} \mathbf{W}^{t,k\top} / \tau_i^t), \quad (8)$$

253 where τ_i^t is introduced to control the smoothness of the curriculum pseudo-label \mathbf{d}_i^t of the
 254 instance \mathbf{x}_i^t , $\mathbf{z}_i^{t,k} \in \mathbb{R}^{1 \times r}$ is a extracted feature vector in the r -dimensional space, and $\mathbf{W}^{t,k} =$
 255 $[\mathbf{w}_1^{t,k}, \mathbf{w}_2^{t,k}, \dots, \mathbf{w}_c^{t,k}]^\top \in \mathbb{R}^{c \times r}$ is the c class prototypes at the k -th curriculum. In our CU-
 256 PLOT framework, we employ a Q -layer neural network with the Softmax operation as the in-
 257 instantiation of the predictive model $f(\cdot; \Theta) = \text{Softmax}(h(\phi(\cdot; \Theta_{1:Q-1}); \Theta_Q))$, where $\Theta_{1:Q-1} =$
 258 $\{\Theta_1, \Theta_2, \dots, \Theta_{Q-1}\}$ denotes the parameters of the feature extractor ϕ , Θ_Q denotes the parameters
 259 of the last linear layer h . Hence, the extracted feature $\mathbf{z}_i^{t,k}$ is calculated by:
 260

$$261 \quad \mathbf{z}_i^{t,k} = \frac{\phi(\mathbf{x}_i^t; \Theta_{1:Q-1}^{t-1,k-1})}{\|\phi(\mathbf{x}_i^t; \Theta_{1:Q-1}^{t-1,k-1})\|_1}, \quad (9)$$

264 where the L1-norm is employed to perform normalization.
 265

266 The j -th class prototype $\mathbf{w}_j^{t,k}$ in $\mathbf{W}^{t,k}$ will be calculated from the extracted features of the selected
 267 instances in the previous curricula:
 268

$$269 \quad \mathbf{w}_j^{t,k} = \frac{\sum_{i=1}^{n^t} \mathbb{I}[\hat{y}_i^t = j] s_i^{t,k} \mathbf{z}_i^{t,k}}{\sum_{i=1}^{n^t} \mathbb{I}[\hat{y}_i^t = j] s_i^{t,k}}, \quad (10)$$

Algorithm 1 The CUPLOT Framework

Input: The pre-trained predictive model $f(\cdot; \Theta^0)$, a sequence of unlabeled mini-batches $\mathcal{D}_{\mathcal{T}}$;

- 1: **for** $t = 1, 2, \dots, T$ **do**
- 2: **for** $k = 1, 2, \dots, K^t$ **do**
- 3: Evaluate the content to be learned through gradient consistency $\mu^{t,k}$ based on Eq. (6);
- 4: Arrange instances into the curriculum content $\mathbf{m}^{t,k}$ according to Eq. (7);
- 5: Generate the curriculum pseudo-label $\mathbf{d}_i^{t,k}$ for each instance based on Eq. (8);
- 6: Optimize the parameters of the model from $\Theta^{t-1,k-1}$ to $\Theta^{t-1,k}$ based on Eq. (3);
- 7: **end for**
- 8: **end for**

Output: The predictive model $f(\cdot; \Theta^T)$.

where $\hat{y}_i^t = \arg \max_{j \in \mathcal{Y}} f_j(\mathbf{x}_i^t; \Theta^{t-1,k-1})$ is the prediction of the model on the instance \mathbf{x}_i^t . Practically, we follow (Wang et al., 2023) to maintain a memory bank to store the pairs of extracted features and outputs of the model, and follow (Iwasawa & Matsuo, 2021) to filter pairs which may be incorrect.

According to Eq. (8), (9), and (10), we build a strong relationship between the pseudo label \mathbf{d} and the sequence matrix of curriculum \mathbf{M}^t , enabling domain knowledge to be absorbed in a more fine-grained manner. The quality of the generated curriculum pseudo-labels improves accordingly, thereby adapting the model to the test domain more effectively. The detailed algorithmic description of CUPLOT is presented in Algorithm 1.

3.3 THEORETICAL ANALYSIS

To demonstrate the superiority of the curriculum framework in OTTA, we first need to define a crucial concept helping us quantify the model’s proximity to the Bayes optimal classifier on target domain.

Definition 1. (e^* -adaptation ability). Let $L(\Theta) := \{\mathbf{x} | y = \arg \max_{j \in \mathcal{Y}} f_j(\mathbf{x}; \Theta)\}$ denote instances predicted correctly by the model f with the parameters Θ , and $L(e) := \{\mathbf{x} | p(y|\mathbf{x}) - p(o|\mathbf{x}) \leq e\}$, where $o = \arg \max_{j \in \mathcal{Y}, j \neq y} p(j|\mathbf{x})$, denote instance whose posterior margin between the highest and second-highest is less than e . We say that the model $f(\cdot; \Theta)$ has the e -adaptation ability on the target domain \mathcal{T} , if $e^* = \arg \max_e |L(\Theta) \cap L(e)|$, where $|\cdot|$ denotes the cardinality of a set.

The value of e can reflect the bound of the model’s approaching the Bayes optimal classifier, provided that Tsybakov condition (Chaudhuri & Dasgupta, 2014; Belkin et al., 2018; Qiao et al., 2019), which quantifies how well classes are separated on the decision boundary $\{\mathbf{x} : p(y|\mathbf{x}) = p(o|\mathbf{x})\}$, is satisfied. Specifically, there exists constants $C, \lambda > 0$, and $\epsilon_0 \in (0, 1)$, such that for all $\epsilon \leq \epsilon_0$, $\mathbb{P}[p(y|\mathbf{x}) - p(o|\mathbf{x}) \leq e] \leq Ce^\lambda$. Then the chance of the model $f(\cdot; \Theta)$ with e^* -adaptation ability to be consistent with the Bayes optimal classifier on the target domain is bounded as follows:

$$\mathbb{P}[\mathbf{x} \in L(\Theta)] \geq 1 - Ce^{*\lambda}, \quad (11)$$

where we employ $O(e^*)$ to denote the above bound.

Next, we establish the relationship between the gradient update and the proportion of correct pseudo-labels. Let Θ^* denote the parameters of a well-adapted classifier under the target domain distribution $p_{\mathcal{T}}(\mathbf{x}, y)$, $\mathcal{I} = \{i | \arg \max_{j \in \mathcal{Y}} d_{i,j} = y_i\}$ denote some instances with correct pseudo-labels, $\bar{\mathcal{I}} = \{i | \arg \max_{j \in \mathcal{Y}} d_{i,j} \neq y_i\}$ denote some instances with incorrect pseudo-labels. We make the following assumption:

Assumption 1. Let $\nabla \Theta(\mathcal{D}) = \sum_{i \in \mathcal{D}} \alpha \frac{\partial \ell(f(\mathbf{x}; \Theta), \mathbf{d}_i)}{\partial \Theta}$ denote the gradient of the model $f(\cdot; \Theta)$ using pseudo-labels on the instances with any index set \mathcal{D} . Then there exists the constant $\zeta > 0$, we have $\|\Theta - \nabla \Theta(\mathcal{D}) - \Theta^*\| \leq \zeta \frac{|\bar{\mathcal{I}} \cap \mathcal{D}|}{|\mathcal{I} \cap \mathcal{D}|}$.

Assumption 1 implies that if Θ is updated using the instances with more correct pseudo-labels in a batch, it will get closer to Θ^* , the parameters of the Bayes optimal classifier. In contrast, if Θ is updated using the instances with more incorrect pseudo-labels in a batch, it will move further away from Θ^* . Then under Assumption 1, we could obtain the following theorem about the bound $O(e^*)$:

324
325
326
Table 1: Classification accuracy (%) and Wilcoxon signed-ranks test results (win[p-value]) of
327
comparing approaches on image corruption benchmarks. Full results are in Tables 17–19.
328

329 330 331 332 333 334 335 336 337 338 339 340 Methods	329 330 331 332 333 334 335 336 337 338 339 340 CIFAR-10-C	329 330 331 332 333 334 335 336 337 338 339 340 CIFAR-100-C	329 330 331 332 333 334 335 336 337 338 339 340 ImageNet-C
329 330 331 332 333 334 335 336 337 338 339 340 ERM	329 330 331 332 333 334 335 336 337 338 339 340 55.51 win[6.1e-5]	329 330 331 332 333 334 335 336 337 338 339 340 34.20 win[6.1e-5]	329 330 331 332 333 334 335 336 337 338 339 340 40.05 win[6.1e-5]
329 330 331 332 333 334 335 336 337 338 339 340 BN	329 330 331 332 333 334 335 336 337 338 339 340 85.48 win[6.5e-4]	329 330 331 332 333 334 335 336 337 338 339 340 56.68 win[6.1e-5]	329 330 331 332 333 334 335 336 337 338 339 340 –
329 330 331 332 333 334 335 336 337 338 339 340 TENT	329 330 331 332 333 334 335 336 337 338 339 340 85.81 win[3.1e-4]	329 330 331 332 333 334 335 336 337 338 339 340 57.21 win[6.1e-5]	329 330 331 332 333 334 335 336 337 338 339 340 –
329 330 331 332 333 334 335 336 337 338 339 340 PL	329 330 331 332 333 334 335 336 337 338 339 340 85.91 win[6.5e-4]	329 330 331 332 333 334 335 336 337 338 339 340 58.44 win[6.1e-5]	329 330 331 332 333 334 335 336 337 338 339 340 49.99 win[6.1e-5]
329 330 331 332 333 334 335 336 337 338 339 340 SHOT-IM	329 330 331 332 333 334 335 336 337 338 339 340 86.33 win[6.1e-5]	329 330 331 332 333 334 335 336 337 338 339 340 59.14 win[1.8e-4]	329 330 331 332 333 334 335 336 337 338 339 340 54.43 win[6.5e-4]
329 330 331 332 333 334 335 336 337 338 339 340 T3A	329 330 331 332 333 334 335 336 337 338 339 340 59.56 win[6.1e-5]	329 330 331 332 333 334 335 336 337 338 339 340 34.89 win[6.1e-5]	329 330 331 332 333 334 335 336 337 338 339 340 39.67 win[6.1e-5]
329 330 331 332 333 334 335 336 337 338 339 340 TAST	329 330 331 332 333 334 335 336 337 338 339 340 85.30 win[6.1e-5]	329 330 331 332 333 334 335 336 337 338 339 340 51.52 win[6.1e-5]	329 330 331 332 333 334 335 336 337 338 339 340 34.67 win[6.1e-5]
329 330 331 332 333 334 335 336 337 338 339 340 TAST-BN	329 330 331 332 333 334 335 336 337 338 339 340 86.11 win[2.2e-3]	329 330 331 332 333 334 335 336 337 338 339 340 50.92 win[6.1e-5]	329 330 331 332 333 334 335 336 337 338 339 340 –
329 330 331 332 333 334 335 336 337 338 339 340 TSD	329 330 331 332 333 334 335 336 337 338 339 340 86.51 win[1.5e-3]	329 330 331 332 333 334 335 336 337 338 339 340 58.49 win[8.0e-4]	329 330 331 332 333 334 335 336 337 338 339 340 44.05 win[6.1e-5]
329 330 331 332 333 334 335 336 337 338 339 340 PROGRAM	329 330 331 332 333 334 335 336 337 338 339 340 82.10 win[6.1e-5]	329 330 331 332 333 334 335 336 337 338 339 340 55.63 win[6.1e-5]	329 330 331 332 333 334 335 336 337 338 339 340 34.45 win[6.1e-5]
329 330 331 332 333 334 335 336 337 338 339 340 DEYO	329 330 331 332 333 334 335 336 337 338 339 340 86.14 win[6.1e-5]	329 330 331 332 333 334 335 336 337 338 339 340 59.08 win[6.5e-4]	329 330 331 332 333 334 335 336 337 338 339 340 50.43 win[6.1e-5]
329 330 331 332 333 334 335 336 337 338 339 340 CUPLOT	329 330 331 332 333 334 335 336 337 338 339 340 87.35	329 330 331 332 333 334 335 336 337 338 339 340 60.11	329 330 331 332 333 334 335 336 337 338 339 340 55.21

341
342
343
344
345
346
Theorem 1. Suppose that the difference between $f_j(\mathbf{x}; \Theta)$ and $p(j|\mathbf{x})$ and the incorrectness of
pseudo-labels is bounded by the distance between Θ and Θ^* , i.e., there exist the constants $\beta, \gamma > 0$,
 $|f_j(\mathbf{x}; \Theta) - p(j|\mathbf{x})| \leq \beta \|\Theta - \Theta^*\|$ and $\frac{|\mathcal{I} \cap \mathcal{D}|}{|\mathcal{I} \cap \mathcal{D}|} \leq \gamma \|\Theta - \Theta^*\|$. Consider an arriving batch \mathcal{D}_T^t ,
the model trained with the pseudo-labels generated at the batch level has e^* -adaptation ability
while another model trained with the pseudo-labels derived from the curriculum framework has
 $e^{* \prime}$ -adaptation ability. Then, under Assumption 1, we could obtain:

$$O(e^{* \prime}) \geq O(e^*). \quad (12)$$

347
348
349
350
351
352
353
354
355
356
357
358
359
The proof of Theorem 1 is provided in Appendix A.1. Theorem 1 shows that the chance of the
model trained with our curriculum pseudo-labels to be consistent with the Bayes optimal classifier
on the target domain could be bounded by a larger lower bound than that of the model trained with
coarse-grained batch-level pseudo-labels. In the proof of Theorem 1, we show that the pseudo-label
error $e^{* \prime}$ obtained under our curriculum-based framework satisfies $e^{* \prime} \leq e^*$, where e^* corresponds to
the batch-level baseline. This inequality rigorously demonstrates that our instance-level curriculum
reduces the effective pseudo-label error, and thus the model under our framework converges to the
Bayes-optimal classifier at a faster rate than the batch-level method.

4 EXPERIMENTS

4.1 DATASETS

360
361
362
363
364
365
366
367
368
369
370
371
Following recent advancements in online test-time adaptation (Jang et al., 2023; Sun et al., 2024),
we evaluate our proposed method using a combination of image corruption benchmark datasets and
domain generalization datasets. Specifically, we employ two widely employed image corruption
benchmarks CIFAR-10-C and CIFAR-100-C (Hendrycks & Dietterich, 2019), and one more
complex dataset ImageNet-C. These datasets introduce 15 types of common corruptions such as
Gaussian noise and motion blurring, which are systematically applied to the test sets of CIFAR-10,
CIFAR-100 and ImageNet-C to evaluate model robustness. For training, we use the original
training sets of CIFAR-10, CIFAR-100 and ImageNet as source domains, while the highest
severity level of corruption in CIFAR-10-C and CIFAR-100-C serves as the target domain. 20%
of the source domain data is reserved for validation purposes.

372
373
374
375
376
377
Beside, we conduct experiments on four domain generalization benchmarks: PACS (Li et al., 2017)
with 9991 samples and 7 classes collected from 4 domains, VLCS (Torralba & Efros, 2011) with
10729 samples and 5 classes collected from 4 domains, OfficeHome (Venkateswara et al., 2017)
with 15588 samples and 65 classes collected from 4 domains, and DomainNet (Peng et al., 2019)
with 586575 samples and 345 classes collected from 6 domains. We designate one domain as the
target and treat the remaining domains as source domains. The validation set follows the same
partitioning strategy as in the image corruption benchmark datasets.

378
379

4.2 BASELINES

380
381
382
383
384
385
386
387
388
389
390
391
392
393
394
395
396
397
398
399
400

We compare the performance of CUPLOT with eleven baselines frequently used for comparison in online TTA: 1) ERM (Vapnik, 1998): A baseline that directly uses the predictions of the pre-trained model on target testing instances without any adaptation. 2) BN (Schneider et al., 2020): A batch-normalization-based approach that replaces the activation statistics computed from source training instances in batch normalization layers with those computed from target testing instances. 3) TENT (Wang et al., 2020): An entropy-minimization-based approach that adapts BN layers by reducing the entropy of model predictions on target domain data. 4) PL (Lee et al., 2013): A pseudo-labeling-based approach that fine-tunes a predictive model by leveraging pseudo-labels inferred from the predictions of the model on target testing instance. 5) SHOT-IM (Liang et al., 2020): A pseudo-labeling-based approach that adapts the source encoding module by maximizing mutual information between intermediate features and classifier outputs. 6) T3A (Iwasawa & Matsuo, 2021): A pseudo-labeling-based approach that generates pseudo labels for target testing instances based on their distances to the estimated class prototypes. 7) TAST (Jang et al., 2023): A pseudo-labeling-based approach that adapts the model by aligning pseudo-labels inferred from the nearest neighbors with those inferred from class prototypes. 8) TAST-BN (Jang et al., 2023): A variation of TAST that adjusts the BN layers to adapt the model instead of updating the adaptation modules. 9) TSD (Wang et al., 2023): A pseudo-labeling-based approach that leverages a memory bank to calculate the pseudo-prototypes for every class and generate pseudo-labels for model refinement. 10) PROGRAM (Sun et al., 2024): A pseudo-labeling-based approach that connects prototypes and test samples in a graph, facilitating effective message passing among them to generate pseudo-labels. 11) DEYO (Lee et al., 2024): An entropy-minimization-based approach that enhances the model by further considering the influence of the object shape on prediction with a newly proposed confidence metric.

401
402
403
404
405
406
407
408
409

The backbone model of each compared method we employ is the same as previous studies (Jang et al., 2023; Sun et al., 2024) on the image corruption benchmark datasets CIFAR-10-C, CIFAR-100-C and domain generalization benchmark datasets. On the image corruption benchmark datasets CIFAR-10-C and CIFAR-100-C, we adopt ResNet-50 as the backbone model. On domain generalization benchmark datasets, we conduct evaluations using ResNet-18 and ResNet-50 architectures (He et al., 2016), both of which are equipped with batch normalization layers (Ioffe, 2015). For ImageNet-C, the ViT-B32 model is used for compared approaches. Since the ViT-B32 model is not equipped with batch normalization layers, we do not report the results on the Batch-normalization-based approaches such as BN, TENT and TAST-BN.

410
411
412
413
414
415
416
417

As for source training, on domain generalization benchmarks, the models are initialized using pre-trained parameters from ImageNet-1K (Russakovsky et al., 2015). The model is updated using the Adam optimizer with the learning rate set to 5×10^{-5} . On the image corruption benchmarks CIFAR-10-C and CIFAR-100-C, we follow (Liu et al., 2021) and pre-train ResNet-50 for 1000 epochs using a combination of the classification task with the standard cross-entropy loss and the instance discrimination task with a self-supervised loss using the SGD optimizer. To balance the two tasks, the weight for the instance discrimination task is set to 0.1. On ImageNet-C, the pre-trained parameters of the ViT-B32 model is provided by the publicly available `timm` library, which is pretrained on ImageNet-1K.

418
419
420
421
422
423
424
425

As for target adapting, the Adam optimizer is employed to update the model parameters, the batch size is set to 128, and the learning rate is selected from the range between 10^{-3} and 10^{-6} . All hyper-parameters for the TTA setting are finalized prior to accessing any test samples. The hyper-parameters for each compared algorithm are selected according to their performance on the previously split validation datasets (Gulrajani & Lopez-Paz, 2021; Wang et al., 2023). Besides, in order to ensure the reliability of our experimental results, we conduct 3 trials with different random seeds for each compared algorithm to calculate mean and standard on domain generalization benchmarks.

426
427

4.3 EXPERIMENTAL RESULTS

428
429
430
431

Tables 1, 2 and 3 comprehensively present a summary of the classification accuracy achieved by each compared approach within the target domains of the benchmark datasets. Note that we do not report the results of Batch-normalization-based approaches such as BN, TENT and TAST-BN on ImageNet-C in Table 1 since the backbone model ViT-B32 is not equipped with batch normalization layers. Also, due to space limitations, we report full results with detailed mean and

432
 433 Table 2: Classification accuracy of comparing ap-
 434 proaches on domain generalization benchmarks
 435 with ResNet-18. Due to the space limit, full re-
 436 sults could be found on Table 20, 22, 24 and 26
 437 in Appendix A.11.

Methods	PACS	VLCS	OfficeHome	DomainNet
ERM	80.08	75.23	62.41	35.74
BN	83.02	68.74	62.11	34.90
TENT	83.28	69.25	62.30	35.36
PL	85.82	74.60	62.54	35.28
SHOT-IM	82.70	70.99	63.62	35.89
T3A	82.26	<u>75.93</u>	<u>63.83</u>	<u>36.29</u>
TAST	84.60	70.88	63.53	35.37
TAST-BN	85.39	75.02	62.33	35.11
TSD	<u>87.48</u>	74.81	63.12	35.50
PROGRAM	82.50	72.35	62.88	35.94
DEYO	86.63	74.05	63.05	35.36
CUPLOT	87.87	76.97	64.55	37.35

447
 448 Table 4: Classification accuracy (mean \pm std) of CUPLOT and its variant CUPLOT-NM on target
 449 domains.

Domain	Backbone	CUPLOT	CUPLOT-NM
ResNet-18	C	99.41\pm0.15	97.25 \pm 0.39
	L	65.61\pm0.50	62.99 \pm 1.24
	S	71.25\pm2.23	69.09 \pm 2.49
	V	71.61\pm1.40	70.22 \pm 1.79
ResNet-50	C	99.18\pm0.59	95.95 \pm 2.74
	L	65.96\pm1.85	62.10 \pm 2.21
	S	74.12\pm2.62	71.15 \pm 2.42
	V	76.50\pm0.61	73.89 \pm 1.38

461 standard deviation in Appendix A.11. The result that achieves the best performance is highlighted in
 462 bold, and the one ranked second is underlined. From Tables 1, 2 and 3, we could conclude: 1) CUPLOT
 463 **significantly** attains the optimal performance among all benchmark datasets and network architectures,
 464 surpassing every compared method. 2) CUPLOT outperforms the second-ranked methods on image
 465 corruption benchmarks, and it yields an average performance increase of 0.84%, 0.97% and 0.78%
 466 on CIFAR-10-C, CIFAR-100-C and ImageNet-C, respectively. 3) CUPLOT steadily boosts the
 467 classifier’s performance on domain generalization benchmarks. Specifically, it realizes an average
 468 enhancement of 1.06% on DomainNet for ResNet-18 and 1.53% on VLCS for ResNet-50.

4.4 WALL-CLOCK TIME AND MEMORY CONSUMPTION ANALYSIS

471 To assess **wall-clock time** and memory consumption, we follow (Song et al., 2023; Cai et al., 2020)
 472 and conduct comparison experiments with baselines that use gradient computation for updates
 473 on the shot noise corruption of the CIFAR-100-C dataset, employing ResNet-50 as the feature
 474 extractor with a batch size of 128. **Since we use gradient consistency to drive the learning order,**
 475 **the backward-passes-per-sample (BPPS) is $\frac{K^t(K^t-1)}{2}$.** More details could be found in Appendix
 476 A.2. The evaluation results are presented in Table 5, which demonstrates that CUPLOT maintains
 477 comparable latency and memory consumption when achieving better performance. Furthermore, we
 478 demonstrate that CUPLOT could retain practical flexibility and trade-off between effectiveness and
 479 efficiency through its curriculum parameter K^t in Appendix A.6.

4.5 EXTENSION TO CONTINUAL TEST-TIME ADAPTATION

483 To assess whether curriculum-based ordering remains effective under non-stationary environment,
 484 we extend CUPLOT to the setting of Continual Test-Time Adaptation by integrating an mean-teacher
 485 (MT) framework for fair comparison. Following the RMTDöbler et al. (2023) protocol on CIFAR-100
 → CIFAR-100-C (severity 5), the results in Table 6 (Appendix A.3) confirms that curriculum-driven

Table 3: Classification accuracy of comparing approaches on domain generalization benchmarks with ResNet-50. Due to the space limit, full results could be found on Table 21, 23, 25 and 27 in Appendix A.11.

Methods	PACS	VLCS	OfficeHome	DomainNet
ERM	85.47	76.64	67.69	43.29
BN	86.09	68.35	67.18	41.54
TENT	86.58	69.08	67.48	42.42
PL	86.13	73.81	67.61	42.38
SHOT-IM	85.35	69.32	67.98	43.46
T3A	86.01	<u>77.41</u>	68.76	<u>44.11</u>
TAST	86.56	68.53	68.70	42.38
TAST-BN	89.23	71.63	68.60	42.49
TSD	<u>91.03</u>	73.82	<u>69.11</u>	42.27
PROGRAM	86.44	68.42	67.99	43.35
DEYO	88.34	70.49	68.25	42.47
CUPLOT	91.11	78.94	70.30	44.98

486 Table 5: Performance Comparison on CIFAR-100-C (shot noise corruption) with ResNet-50, includ-
 487 ing average wall-clock time, accuracy and memory usage.

489 Methods	490 Wall-Clock Time (s)	491 Params (MB)	492 Activations (MB)	493 Total (MB)	494 Accuracy (%)
TENT	5.15	94.82	1761.61	5517.30	56.33
SHOT-IM	6.86	94.82	3517.50	5801.62	58.24
DEYO	8.21	94.82	3517.50	5990.18	58.06
CUPLOT	8.58	94.82	3517.50	6142.76	59.24

495
 496
 497 ordering is complementary to MT-style temporal ensembling: while EMA stabilizes predictions over
 498 time, ordering controls how fine-grained domain knowledge is absorbed, and the two mechanisms
 499 jointly yield more robust online adaptation.

501 4.6 FURTHER ANALYSIS

502
 503 To verify the effectiveness of the curriculum pseudo-labels in CUPLOT, we carry out an ablation
 504 study with a variant of CUPLOT, i.e., CUPLOT-NM, where the model directly learns the batch without
 505 arranging curricula by setting the threshold $\delta = \min_i \mu^{t,1}$ and the curriculum number $K^t = 1$. As
 506 presented in Table 4, CUPLOT surpasses CUPLOT-NM across all target domains of the PACS dataset
 507 whenever using ResNet-18 and ResNet-50. More ablation details about the selection of consistency
 508 metric could be found in Appendix A.8.

509 Besides, we perform sensitivity analysis to examine the impact of the temperature hyper-parameter
 510 τ in the generation of pseudo-labels in Eq. (8), and the batch size in our framework using the shot
 511 noise corruption of CIFAR-10-C dataset. τ increases from 0.3 to 10, and the batch size varies
 512 from 16 to 256. As illustrated in Figure 2(a), the performance of CUPLOT remains relatively stable
 513 across a broad range, which demonstrates highly desirable robustness to deliver reliable test-time
 514 adaptation performance. Meanwhile, Figure 2(b) presents the average accuracy of various methods
 515 across different batch sizes on shot noise corruption of CIFAR-10-C dataset. From Figure 2(b), our
 516 approach consistently outperforms the other methods under varying batch sizes, which demonstrates
 517 CUPLOT could flexibly handle streaming real-world data of various sizes.

518 Furthermore, our proposed framework provides a novel insight into active OTTA. Different from
 519 the previous active TTA work (Gui et al., 2024), in which human experts work at the aspect of the
 520 label, CUPLOT could bring the active query at the aspect of the instance via providing the difficulty
 521 levels of domain knowledge absorption between instances. Figure 2(c) presents the test accuracy
 522 (y-axis) of a variant of CUPLOT, i.e., CUPLOT-AT on CIFAR-10-C and CIFAR-100-C, where
 523 the different severity levels of corruption are mixed to serve as the target domain, and CUPLOT-AT
 524 has access to the difficulty levels of a certain proportion of data (x-axis). CUPLOT-AT arranges the
 525 data with lower difficulty levels in the earlier curricula for priority learning as much as possible. As
 526 illustrated in Figure 2(c), the performance of our framework could be further improved when the
 527 human experts provide information on the aspect of the instance if the difficulty levels of a larger
 528 proportion of instances are known, which is a nice property for those that require human interaction
 529 to improve the designed algorithm.

530 5 CONCLUSION

531
 532 In this study, we proposed the CUPLOT, a novel online test-time adaptation framework, aiming to
 533 address the issue that most existing Online Test-Time Adaptation (OTTA) methods only exploit
 534 domain knowledge at a coarse-grained batch level. CUPLOT mines domain knowledge at a fine-
 535 grained instance level by organizing the arrived batch into a series of curricula based on the modeled
 536 relevance of domain knowledge between the model and instances, and enabling the model to learn
 537 instances in an orderly manner using pseudo-labels generated by class prototypes. Theoretically, we
 538 demonstrated that the model trained with curriculum pseudo-labels has a larger lower bound of the
 539 probability of being consistent with the Bayes optimal classifier on the target domain, indicating
 stronger adaptation ability. Extensive experiments verify the effectiveness of our proposed framework.

540 REFERENCES

541

542 Emmanuel Abbe, Elisabetta Cornacchia, and Aryo Lotfi. Provable advantage of curriculum learning
543 on parity targets with mixed inputs. *Advances in Neural Information Processing Systems*, 36:
544 24291–24321, 2023.

545 Sherwin Bahmani, Oliver Hahn, Eduard Zamfir, Nikita Araslanov, Daniel Cremers, and Stefan Roth.
546 Semantic self-adaptation: Enhancing generalization with a single sample. *Trans. Mach. Learn.
547 Res. (TMLR)*, 2023.

548 Mikhail Belkin, Daniel J Hsu, and Partha Mitra. Overfitting or perfect fitting? risk bounds for
549 classification and regression rules that interpolate. *Advances in neural information processing
550 systems*, 31, 2018.

551

552 Shai Ben-David, John Blitzer, Koby Crammer, Alex Kulesza, Fernando Pereira, and Jennifer Wortman
553 Vaughan. A theory of learning from different domains. *Mach. Learn.*, 79(1-2):151–175, 2010.

554

555 Yoshua Bengio, Jérôme Louradour, Ronan Collobert, and Jason Weston. Curriculum learning. In
556 *Proceedings of the 26th Annual International Conference on Machine Learning, ICML 2009,
557 Montreal, Quebec, Canada, June 14-18, 2009*, volume 382, pp. 41–48, 2009.

558

559 Malik Boudiaf, Romain Mueller, Ismail Ben Ayed, and Luca Bertinetto. Parameter-free online
560 test-time adaptation. In *Proceedings of the IEEE/CVF Conference on Computer Vision and Pattern
Recognition*, pp. 8344–8353, 2022.

561

562 Han Cai, Chuang Gan, Ligeng Zhu, and Song Han. Tinylt: Reduce memory, not parameters for
563 efficient on-device learning. In *Advances in Neural Information Processing Systems* 33, pp.
564 11285–11297, Virtual Event, 2020.

565

566 Kamalika Chaudhuri and Sanjoy Dasgupta. Rates of convergence for nearest neighbor classification.
567 *Advances in Neural Information Processing Systems*, 27, 2014.

568

569 Mario Döbler, Robert A Marsden, and Bin Yang. Robust mean teacher for continual and gradual
570 test-time adaptation. In *Proceedings of the IEEE/CVF Conference on Computer Vision and Pattern
Recognition*, pp. 7704–7714, 2023.

571

572 Taesik Gong, Jongheon Jeong, Taewon Kim, Yewon Kim, Jinwoo Shin, and Sung-Ju Lee. NOTE: ro-
573 bust continual test-time adaptation against temporal correlation. In *Advances in Neural Information
574 Processing Systems (NeurIPS)*, volume 35, pp. 27253–27266, 2022.

575

576 Sachin Goyal, Mingjie Sun, Aditi Raghunathan, and J. Zico Kolter. Test time adaptation via conjugate
577 pseudo-labels. In *Advances in Neural Information Processing Systems (NeurIPS)*, volume 35, pp.
578 6204–6218, 2022.

579

580 Shurui Gui, Xiner Li, and Shuiwang Ji. Active test-time adaptation: Theoretical analyses and an
581 algorithm. In *The Twelfth International Conference on Learning Representations, ICLR 2024,
582 Vienna, Austria, May 7-11, 2024*, 2024.

583

584 Ishaan Gulrajani and David Lopez-Paz. In search of lost domain generalization. In *9th International
585 Conference on Learning Representations (ICLR)*, 2021.

586

587 Kaiming He, Xiangyu Zhang, Shaoqing Ren, and Jian Sun. Deep residual learning for image
588 recognition. In *Proceedings of the IEEE conference on computer vision and pattern recognition*,
589 pp. 770–778, 2016.

590

591 Yufan He, Aaron Carass, Lianrui Zuo, Blake E. Dewey, and Jerry L. Prince. Autoencoder based
592 self-supervised test-time adaptation for medical image analysis. *Medical Image Anal.*, 72:102136,
593 2021.

594

595 Dan Hendrycks and Thomas Dietterich. Benchmarking neural network robustness to common
596 corruptions and perturbations. *arXiv preprint arXiv:1903.12261*, 2019.

597

598 Sheng-Jun Huang, Rong Jin, and Zhi-Hua Zhou. Active learning by querying informative and
599 representative examples. *Advances in neural information processing systems*, 23, 2010.

594 Aaron Courville Ian Goodfellow, Yoshua Bengio and Yoshua Bengio. *Deep learning*. MIT press,
 595 2016.

596

597 Sergey Ioffe. Batch normalization: Accelerating deep network training by reducing internal covariate
 598 shift. *arXiv preprint arXiv:1502.03167*, 2015.

599

600 Yusuke Iwasawa and Yutaka Matsuo. Test-time classifier adjustment module for model-agnostic
 601 domain generalization. *Advances in Neural Information Processing Systems*, 34:2427–2440, 2021.

602

603 Minguk Jang, Sae-Young Chung, and Hye Won Chung. Test-time adaptation via self-training with
 604 nearest neighbor information. In *The Eleventh International Conference on Learning Representa-
 tions*, 2023.

605

606 Mengmeng Jing, Xiantong Zhen, Jingjing Li, and Cees Snoek. Variational model perturbation for
 607 source-free domain adaptation. In *Advances in Neural Information Processing Systems (NeurIPS)*,
 608 volume 35, pp. 17173–17187, 2022.

609

610 Nazmul Karim, Niluthpol Chowdhury Mithun, Abhinav Rajvanshi, Han-pang Chiu, Supun Sama-
 611 rasekera, and Nazanin Rahnavaard. C-sfda: A curriculum learning aided self-training framework for
 612 efficient source free domain adaptation. In *Proceedings of the IEEE/CVF conference on computer
 vision and pattern recognition*, pp. 24120–24131, 2023.

613

614 Jangho Kim, Juntae Lee, Simyung Chang, and Nojun Kwak. Variational on-the-fly personalization.
 615 In *International Conference on Machine Learning (ICML)*, volume 162, pp. 11134–11147, 2022.

616

617 M. Pawan Kumar, Benjamin Packer, and Daphne Koller. Self-paced learning for latent variable
 618 models. In *Advances in Neural Information Processing Systems 23: 24th Annual Conference on
 619 Neural Information Processing Systems 2010. Proceedings of a meeting held 6-9 December 2010,
 Vancouver, British Columbia, Canada*, pp. 1189–1197, 2010.

620

621 Dong-Hyun Lee et al. Pseudo-label: The simple and efficient semi-supervised learning method for
 622 deep neural networks. In *Workshop on challenges in representation learning, ICML*, volume 3, pp.
 623 896. Atlanta, 2013.

624

625 Jonghyun Lee, Dahuin Jung, Saehyung Lee, Junsung Park, Juhyeon Shin, Uiwon Hwang, and Sungroh
 626 Yoon. Entropy is not enough for test-time adaptation: From the perspective of disentangled factors.
 627 *arXiv preprint arXiv:2403.07366*, 2024.

628

629 Da Li, Yongxin Yang, Yi-Zhe Song, and Timothy M Hospedales. Deeper, broader and artier domain
 630 generalization. In *Proceedings of the IEEE international conference on computer vision*, pp.
 5542–5550, 2017.

631

632 Jian Liang, Dapeng Hu, and Jiashi Feng. Do we really need to access the source data? source
 633 hypothesis transfer for unsupervised domain adaptation. In *International conference on machine
 learning*, pp. 6028–6039. PMLR, 2020.

634

635 Guan-Ting Lin, Shang-Wen Li, and Hung-yi Lee. Listen, adapt, better WER: source-free single-
 636 utterance test-time adaptation for automatic speech recognition. In Hanseok Ko and John H. L.
 637 Hansen (eds.), *23rd Annual Conference of the International Speech Communication Association
 (INTERSPEECH)*, pp. 2198–2202, 2022.

638

639 Yuejiang Liu, Parth Kothari, Bastien Van Delft, Baptiste Bellot-Gurlet, Taylor Mordan, and Alexandre
 640 Alahi. Ttt++: When does self-supervised test-time training fail or thrive? *Advances in Neural
 641 Information Processing Systems*, 34:21808–21820, 2021.

642

643 Zhihe Lu, Yongxin Yang, Xiatian Zhu, Cong Liu, Yi-Zhe Song, and Tao Xiang. Stochastic classifiers
 644 for unsupervised domain adaptation. In *2020 IEEE/CVF Conference on Computer Vision and
 645 Pattern Recognition, CVPR 2020, Seattle, WA, USA, June 13-19, 2020*, pp. 9108–9117, 2020.

646

647 Wenao Ma, Cheng Chen, Shuang Zheng, Jing Qin, Huimao Zhang, and Qi Dou. Test-time adaptation
 648 with calibration of medical image classification nets for label distribution shift. In *Medical Image
 Computing and Computer Assisted Intervention (MICCAI)*, volume 13433, pp. 313–323, 2022.

648 Muhammad Jehanzeb Mirza, Jakub Micorek, Horst Possegger, and Horst Bischof. The norm must
 649 go on: Dynamic unsupervised domain adaptation by normalization. In *IEEE/CVF Conference on*
 650 *Computer Vision and Pattern Recognition (CVPR)*, pp. 14745–14755, 2022.

651 Shuaicheng Niu, Jiaxiang Wu, Yifan Zhang, Zhiqian Wen, Yaofu Chen, Peilin Zhao, and Mingkui
 652 Tan. Towards stable test-time adaptation in dynamic wild world. In *The Eleventh International*
 653 *Conference on Learning Representations (ICLR)*, 2023.

654 Xingchao Peng, Qinxun Bai, Xide Xia, Zijun Huang, Kate Saenko, and Bo Wang. Moment matching
 655 for multi-source domain adaptation. In *Proceedings of the IEEE/CVF international conference on*
 656 *computer vision*, pp. 1406–1415, 2019.

657 Xingye Qiao, Jie Xin Duan, and Guang Cheng. Rates of convergence for large-scale nearest neighbor
 658 classification. *Advances in neural information processing systems*, 32, 2019.

659 Olga Russakovsky, Jia Deng, Hao Su, Jonathan Krause, Sanjeev Satheesh, Sean Ma, Zhiheng Huang,
 660 Andrej Karpathy, Aditya Khosla, Michael Bernstein, et al. Imagenet large scale visual recognition
 661 challenge. *International journal of computer vision*, 115:211–252, 2015.

662 Kate Saenko, Brian Kulis, Mario Fritz, and Trevor Darrell. Adapting visual category models to
 663 new domains. In *Computer Vision - ECCV 2010, 11th European Conference on Computer Vision,*
 664 *Heraklion, Crete, Greece, September 5-11, 2010, Proceedings, Part IV*, volume 6314, pp. 213–226,
 665 2010.

666 Steffen Schneider, Evgenia Rusak, Luisa Eck, Oliver Bringmann, Wieland Brendel, and Matthias
 667 Bethge. Improving robustness against common corruptions by covariate shift adaptation. *Advances*
 668 *in neural information processing systems*, 33:11539–11551, 2020.

669 Inkyu Shin, Yi-Hsuan Tsai, Bingbing Zhuang, Samuel Schulter, Buyu Liu, Sparsh Garg, In So Kweon,
 670 and Kuk-Jin Yoon. MM-TTA: multi-modal test-time adaptation for 3d semantic segmentation. In
 671 *IEEE/CVF Conference on Computer Vision and Pattern Recognition (CVPR)*, pp. 16907–16916,
 672 2022.

673 Guohao Chen, Pengcheng Wu, Peilin Zhao, Shuaicheng Niu, Chunyan Miao. Test-time model adapta-
 674 tion with only forward passes. In *Proceedings of the 41st International Conference on Machine*
 675 *Learning, Vienna, Austria*, 2024.

676 Damian Sójka, Sebastian Cygert, Bartłomiej Twardowski, and Tomasz Trzcinski. Ar-tta: A simple
 677 method for real-world continual test-time adaptation. In *Proceedings of the IEEE/CVF International*
 678 *Conference on Computer Vision*, pp. 3491–3495, 2023.

679 Junha Song, Jungsoo Lee, In So Kweon, and Sungha Choi. Ecotta: Memory-efficient continual test-
 680 time adaptation via self-distilled regularization. In *Proceedings of the 2023 IEEE/CVF Conference*
 681 *on Computer Vision and Pattern Recognition*, pp. 11920–11929, Vancouver, Canada, 2023.

682 Haopeng Sun, Lumin Xu, Sheng Jin, Ping Luo, Chen Qian, and Wentao Liu. Program: Prototype
 683 graph model based pseudo-label learning for test-time adaptation. In *The Twelfth International*
 684 *Conference on Learning Representations*, 2024.

685 Antonio Torralba and Alexei A Efros. Unbiased look at dataset bias. In *CVPR 2011*, pp. 1521–1528.
 686 IEEE, 2011.

687 Laurens Van der Maaten and Geoffrey Hinton. Visualizing data using t-sne. *Journal of machine*
 688 *learning research*, 9(11), 2008.

689 Vladimir Vapnik. Statistical learning theory. *John Wiley & Sons google schola*, 2:831–842, 1998.

690 Hemanth Venkateswara, Jose Eusebio, Shayok Chakraborty, and Sethuraman Panchanathan. Deep
 691 hashing network for unsupervised domain adaptation. In *Proceedings of the IEEE conference on*
 692 *computer vision and pattern recognition*, pp. 5018–5027, 2017.

693 Riccardo Volpi, Pau de Jorge, Diane Larlus, and Gabriela Csurka. On the road to online adaptation
 694 for semantic image segmentation. In *IEEE/CVF Conference on Computer Vision and Pattern*
 695 *Recognition (CVPR)*, pp. 19162–19173, 2022.

702 Dequan Wang, Evan Shelhamer, Shaoteng Liu, Bruno Olshausen, and Trevor Darrell. Tent: Fully
 703 test-time adaptation by entropy minimization. *arXiv preprint arXiv:2006.10726*, 2020.

704

705 Qin Wang, Olga Fink, Luc Van Gool, and Dengxin Dai. Continual test-time domain adaptation.
 706 In *Proceedings of the IEEE/CVF Conference on Computer Vision and Pattern Recognition*, pp.
 707 7201–7211, 2022.

708

709 Shuai Wang, Daoan Zhang, Zipei Yan, Jianguo Zhang, and Rui Li. Feature alignment and uniformity
 710 for test time adaptation. In *Proceedings of the IEEE/CVF Conference on Computer Vision and*
 711 *Pattern Recognition*, pp. 20050–20060, 2023.

712

713 Songbai Yan, Kamalika Chaudhuri, and Tara Javidi. Active learning from imperfect labelers. *Ad-*
 714 *vances in neural information processing systems*, 29, 2016.

715

716 Hongzheng Yang, Cheng Chen, Meirui Jiang, Quande Liu, Jianfeng Cao, Pheng-Ann Heng, and
 717 Qi Dou. DLTTA: dynamic learning rate for test-time adaptation on cross-domain medical images.
 718 *IEEE Trans. Medical Imaging (TMI)*, 41(12):3575–3586, 2022.

719

720 Zhuang Liu, John Miller, Alexei A. Efros, Moritz Hardt, Yu Sun, Xiaolong Wang. Test-time training
 721 with self-supervision for generalization under distribution shifts. In *Proceedings of the 37th*
 722 *International Conference on Machine Learning, Virtual Event*, 2020.

723

724 Bowen Zhang, Yidong Wang, Wenxin Hou, Hao Wu, Jindong Wang, Manabu Okumura, and Takahiro
 725 Shinozaki. Flexmatch: Boosting semi-supervised learning with curriculum pseudo labeling.
 726 *Advances in neural information processing systems*, 34:18408–18419, 2021.

727

728 Marvin Zhang, Sergey Levine, and Chelsea Finn. MEMO: test time robustness via adaptation and
 729 augmentation. In *Advances in Neural Information Processing Systems (NeurIPS)*, volume 35, pp.
 730 38629–38642, 2022.

731

732 Bowen Zhao, Chen Chen, and Shu-Tao Xia. Delta: Degradation-free fully test-time adaptation. In
 733 *Proceedings of the 11th International Conference on Learning Representations, Kigali, Rwanda*,
 734 2023.

735

736 Tianyi Zhou, Shengjie Wang, and Jeff Bilmes. Robust curriculum learning: from clean label detection
 737 to noisy label self-correction. In *International conference on learning representations*, 2020a.

738

739 Tianyi Zhou, Shengjie Wang, and Jeffrey Bilmes. Curriculum learning by dynamic instance hardness.
 740 *Advances in Neural Information Processing Systems*, 33:8602–8613, 2020b.

741

742

743

744

745

746

747

748

749

750

751

752

753

754

755

A TECHNICAL APPENDICES AND SUPPLEMENTARY MATERIAL

A.1 PROOFS OF THEOREM 1

Theorem 1. Suppose that the difference between $f_j(\mathbf{x}; \Theta)$ and $p(j|\mathbf{x})$ and the incorrectness of pseudo-labels is bounded by the distance between Θ and Θ^* , i.e., there exist the constants $\beta, \gamma > 0$, $|f_j(\mathbf{x}; \Theta) - p(j|\mathbf{x})| \leq \beta \|\Theta - \Theta^*\|$ and $\frac{|\mathcal{I} \cap \mathcal{D}|}{|\mathcal{I} \cap \mathcal{D}|} \leq \gamma \|\Theta - \Theta^*\|$. Consider an arriving batch \mathcal{D}_T^t , the model trained with the pseudo-labels generated at the batch level has e^* -adaptation ability while another model trained with the pseudo-labels derived from the curriculum framework has $e^{* \prime}$ -adaptation ability. Then, under Assumption 1, we could obtain:

$$O(e^{* \prime}) \geq O(e^*).$$

Proof. We start by clarifying the key concepts and notations relevant to the proof. According to Definition 1, the e^* -adaptation ability of the model $f(\cdot; \Theta)$ is determined by $e^* = \arg \max_e |L(\Theta) \cap L(e)|$, and we know that $\mathbb{P}[\mathbf{x} \in L(\Theta)] \geq 1 - Ce^{*\lambda} = O(e^*)$. To prove $O(e^{* \prime}) \geq O(e^*)$, we aim to show that $e^{* \prime} \leq e^*$ since $O(e)$ is a decreasing function of e . Here, e^* corresponds to the model trained with batch-level pseudo-labels, and $e^{* \prime}$ corresponds to the model trained with curriculum-framework pseudo-labels.

First, we analyze the difference in model predictions. Given the condition $|f_j(\mathbf{x}; \Theta) - p(j|\mathbf{x})| \leq \beta \|\Theta - \Theta^*\|$, consider the model trained with curriculum-framework pseudo-labels $f(\cdot; \Theta_{\text{curriculum}})$ and the model trained with batch-level pseudo-labels $f(\cdot; \Theta_{\text{batch}})$.

Next, we show that the curriculum framework can make better use of correct pseudo-labeled samples. Let \mathcal{D}^k be the cumulative instances in the curriculum framework. From the perspective of parameter update, since the curriculum-framework model is closer to Θ^* at the $k-1$ -th step, according to the inequality $\|\Theta - \nabla \Theta(\mathcal{D}^{k-1}) - \Theta^*\| \leq \zeta \frac{|\mathcal{I} \cap \mathcal{D}^{k-1}|}{|\mathcal{I} \cap \mathcal{D}^{k-1}|}$ in Assumption 1, when the update is carried out at the k -th step, $\frac{|\mathcal{I} \cap \mathcal{D}^k|}{|\mathcal{I} \cap \mathcal{D}^k|}$ will further get smaller and the curriculum-framework model will further narrow the distance from Θ^* , that is, $\|\Theta_{\text{curriculum}}^k - \Theta^*\| \leq \|\Theta_{\text{curriculum}}^{k-1} - \Theta^*\|$. This implies that the curriculum-framework model can make better use of correct pseudo-labeled samples by setting reasonable curriculum number. By Assumption 1, updating with more correct pseudo-labels makes the model further approach Θ^* . Thus, we have

$$\|\Theta_{\text{curriculum}} - \Theta^*\| \leq \|\Theta_{\text{batch}} - \Theta^*\|. \quad (13)$$

From this, we can infer that

$$|f_j(\mathbf{x}; \Theta_{\text{curriculum}}) - p(j|\mathbf{x})| \leq |f_j(\mathbf{x}; \Theta_{\text{batch}}) - p(j|\mathbf{x})|, \quad (14)$$

which indicates that the predictions of the model trained with the curriculum framework are closer to the true probability distribution $p(j|\mathbf{x})$.

We analyze the difference in the error rates of pseudo-labels. According to $\frac{|\mathcal{I} \cap \mathcal{D}|}{|\mathcal{I} \cap \mathcal{D}|} \leq \gamma \|\Theta - \Theta^*\|$, because $\|\Theta_{\text{curriculum}} - \Theta^*\| \leq \|\Theta_{\text{batch}} - \Theta^*\|$, the error rate of pseudo-labels in the curriculum-framework training is lower. That is, the proportion of mislabeled samples in the total samples for the model trained with the curriculum framework is smaller.

Then, we combine the above-mentioned facts with the definition to derive the inequality. According to Definition 1, $L(\Theta) = \{\mathbf{x} | y = \arg \max_{j \in \mathcal{Y}} f_j(\mathbf{x}; \Theta)\}$ and $L(e) = \{\mathbf{x} | p(y|\mathbf{x}) - p(o|\mathbf{x}) \leq e\}$. Since the model trained with the curriculum framework has more accurate predictions and a lower error rate of pseudo-labels, the number of instances that satisfy both $y = \arg \max_{j \in \mathcal{Y}} f_j(\mathbf{x}; \Theta_{\text{curriculum}})$ and $p(y|\mathbf{x}) - p(o|\mathbf{x}) \leq e$ is relatively larger.

Specifically, we have

$$|L(\Theta_{\text{curriculum}}) \cap L(e)| \geq |L(\Theta_{\text{batch}}) \cap L(e)|. \quad (15)$$

When calculating $e^* = \arg \max_e |L(\Theta) \cap L(e)|$, for the model trained with the curriculum framework, $e^{* \prime}$ makes $|L(\Theta_{\text{curriculum}}) \cap L(e^{* \prime})|$ reach its maximum value. And because

$$|L(\Theta_{\text{curriculum}}) \cap L(e^{* \prime})| \geq |L(\Theta_{\text{batch}}) \cap L(e^*)|, \quad (16)$$

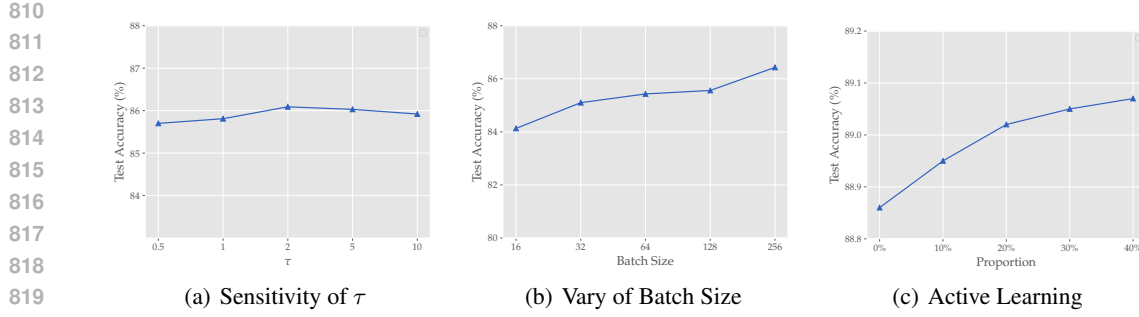


Figure 2: The parameter sensitivity analysis for CUPLOT.

Table 9: GPU time and classification accuracy induced by curriculum learning with varying K^t on shot noise of CIFAR-10-C.

K^t	1	2	3	4
Time	6.10	7.55	8.37	8.97
Acc.	85.04	86.06	86.21	86.45

Table 10: GPU time and classification accuracy induced by curriculum learning with varying K^t on clipart subset of DomainNet.

K^t	1	2	3	4
Time	102.18	113.32	126.59	137.38
Acc.	50.82	51.77	51.89	52.07

we can conclude that

$$e^{\star'} \leq e^{\star}. \quad (17)$$

Finally, since $O(e^{\star}) = 1 - Ce^{\star\lambda}$ is a monotonically decreasing function of e , we can obtain $O(e^{\star'}) \geq O(e^{\star})$. Therefore, Theorem 1 is proved.

Table 6: Classification **error rate** (%) on the CIFAR-100 \rightarrow CIFAR-100-C online continual test-time adaptation task under the highest corruption severity level (severity 5), evaluated on ResNeXt-29 following the Döbler et al. (2023) protocol.

Methods	Gaussian	shot	impulse	defocus	glass	motion	zoom	snow	frost	fog	brightness	contrast	elastic	pixelate	jpeg	Mean
Source	73.0	68.0	39.4	29.3	54.1	30.8	28.9	39.5	45.8	50.3	29.5	55.1	37.2	74.7	41.2	46.4
BN	42.1	40.7	42.7	27.6	41.9	29.7	27.9	34.9	35.0	41.5	26.5	30.3	35.7	32.9	41.2	35.4
TENT	37.2	35.8	41.7	37.9	51.2	48.3	45.8	58.4	63.7	71.1	70.4	82.3	88.0	88.5	90.4	60.9
CoTTA	40.1	37.7	39.7	26.9	38.0	27.9	26.4	32.8	31.8	40.3	24.7	26.9	32.5	28.3	33.5	32.5
RMT	38.5	34.4	35.4	26.4	32.7	27.0	25.0	27.6	27.5	30.0	24.0	25.8	27.0	25.2	28.4	29.0
Ours	38.0	34.0	34.8	26.0	32.2	26.4	24.5	27.2	27.1	29.5	23.5	25.3	26.6	24.7	27.9	28.5

A.2 WALL-CLOCK TIME AND MEMORY CONSUMPTION ANALYSIS

We measured the **wall-clock time** and memory usage of our approach and baselines following EcoTTA (Song et al., 2023). Specifically, all methods are performed on a CPU constrained to 2 cores and 4 threads to emulate computationally constrained scenarios. We measured the average **wall-clock** time per batch using `time.perf_counter`, recording the wall-clock time before and after the execution of the TTA algorithm and averaging over all batches. The parameter and activation memory costs are measured following the TinyTL (Cai et al., 2020) codebase, and the total memory usage is tracked via `memory_profiler.memory_usage` with an interval of 0.01 seconds. The results are shown in Table 5.

A.3 EXTENSION TO CONTINUAL TEST-TIME ADAPTATION

To examine whether curriculum-based ordering remains beneficial under strong Mean-Teacher (MT)-style stabilization, we further extend CUPLOT to Continual Test-Time Adaptation by integrating an EMA teacher into our adaptation pipeline. MT-based approaches such as COTTA (Wang et al. (2022) and RMT (Döbler et al. (2023) stabilize online adaptation by smoothing predictions over time via teacher-student consistency. Since our curriculum mechanism is orthogonal to this

Table 7: Classification accuracy of active learning variants on CIFAR-10-M35.

Sampling Rate	10%	20%	0.3%	0.4%
CUPLOT-AT	86.62	86.72	86.83	86.96
CUPLOT-E	86.56	86.64	86.70	86.77
CUPLOT-G	86.53	86.62	86.69	86.75
CUPLOT-M	86.53	86.59	86.66	86.71

Table 8: Classification accuracy of our approach and compared methods on real-world temporal-shift datasets.

Dataset	ERM	BN	TENT	PL	SHOT-IM	TSD	CUPLOT
Yearbook	81.30	84.54	84.53	84.67	85.17	85.11	85.53
EVIS	56.59	45.72	45.73	45.78	45.93	46.01	56.87

stabilization—targeting the ordering of incoming samples rather than temporal ensembling—we evaluate whether ordering still brings improvements when combined with an EMA teacher.

Following the Döbler et al. (2023) evaluation protocol, we conduct experiments on the CIFAR-100 → CIFAR-100-C continual test-time adaptation task at corruption severity 5 using ResNeXt-29. Table 6 reports classification error rates across all 15 corruption types. These results demonstrate that ordering benefits do not vanish under MT-style smoothing; instead, EMA-based prediction averaging and curriculum-driven sample ordering are complementary, providing cumulative improvements in adaptation stability and accuracy.

A.4 COMPARISON TO COMMON ACTIVE LEARNING STRATEGIES

We conducted additional experiments comparing CUPLOT-AT (gradient-consistency-based instance selection) against three active learning variants equipped with different sampling criteria commonly used active learning (Huang et al., 2010; Yan et al., 2016), including:

- CUPLOT-E (entropy-based): $\text{Score}(x_i) = \sum_{j=1}^C d_i^j \log d_i^j$,
- CUPLOT-G (margin-based): $\text{Score} = d_i^m - d_i^o$, where $m = \arg \max_{j \in \mathcal{Y}} d_i^j$ and $o = \arg \max_{j \in \mathcal{Y}, j \neq m} d_i^j$.
- CUPLOT-M (maximum-based): $\text{Score} = d_i^m$

Similar to CUPLOT-AT, samples with higher scores are prioritized for earlier curricula, while those with lower scores are scheduled for later curricula. We manually create a dataset CIFAR-10-M35 by mixing samples from CIFAR-10-C with difficulty levels 3 and 5. Table 7 illustrates the performance of these active learning variants on CIFAR-10-M35. From Table 7, we could observe the superiority of gradient-consistency-based instance selection.

Table 11: Classification accuracy of our approach and compared methods on shot noise of CIFAR-10-C under different batch sizes.

Methods	2	4	8	16	32	64	128	256	512
SHOT-IM	63.17	72.32	78.43	82.13	83.62	85.00	85.04	84.41	85.61
DEYO	63.77	72.93	79.08	82.35	83.86	84.82	84.58	84.87	85.09
CUPLOT	66.87	74.40	80.42	84.01	85.03	85.93	86.06	85.97	86.15

918 Table 12: Classification accuracy of different consistency metrics on CIFAR-100-C.
919

Criterion	Noise	Blur	Weather	Digital
Gradient Consistency	55.16	64.01	58.80	62.70
Uncertainty	54.79	63.76	58.66	62.55
Cross-entropy Loss	54.85	63.69	58.63	62.61

925
926 Table 13: Classification accuracy of different consistency metrics on PACS.
927

Criterion	A	C	P	S
Gradient Consistency	91.33	90.00	97.60	85.51
Uncertainty	90.92	89.84	97.68	85.22
Cross-entropy Loss	90.81	89.95	97.55	85.15

935 A.5 PRACTICAL APPLICABILITY OF OUR METHOD
936937 To assess CUPLOT’s real-world applicability, we conducted additional experiments on two temporal-
938 shift datasets that reflect natural, non-synthetic distribution shifts:
939940

941 - Yearbook: A long-span dataset of high school portraits spanning eight decades, characterized by
evolving demographics, camera technologies, and visual styles.
942 - EVIS: A dataset of electronic product and vehicle images, indexed by upload dates to capture
real-world trends and domain drift.
943
944 These datasets simulate realistic test-time adaptation scenarios where the target domain shifts over
945 time and is not seen during training. As shown below in Table 8, CUPLOT significantly outperforms
946 existing TTA methods, demonstrating its ability to generalize and adapt in complex real-life settings.
947948 A.6 TRADE-OFF BETWEEN EFFECTIVENESS AND EFFICIENCY
949950 CUPLOT retains practical flexibility and trade-off between effectiveness and efficiency through its
951 curriculum parameter K^t (number of curricula per batch), empirically defined as $K^t = \text{round}(\log n^t)$
952 by default. Reducing K^t (e.g., setting $K^t = 1$ to mimic batch-level learning) significantly lowers
953 computational cost while retaining performance gains to some extent. This allows users to tailor K^t to
954 resource constraints, balancing efficiency and accuracy. Table 9 and Table 10 report the running time
955 when K^t varies from $[1, 4]$ on CIFAR-10-C using ResNet-50 and DomainNet using ResNet-18,
956 demonstrating CUPLOT’s practical flexibility and trade-off between effectiveness and efficiency.
957958 A.7 CUPLOT’S PERFORMANCE UNDER VARYING BATCH SIZES
959960 Table 11 presents the classification accuracy of our approach and compared methods on shot noise
961 of CIFAR-10-C under different batch sizes. These results demonstrate that our method achieves
962 consistently high accuracy across a wide range of batch sizes.
963964 A.8 PERFORMANCE WITH OTHER METRICS
965966 We conducted ablation studies comparing gradient consistency with entropy. Table 12 and 13 presents
967 the accuracy of different metrics on CIFAR-100-C and PACS, respectively. From the tables, we
968 validate the effectiveness of gradient consistency compared to entropy.
969970 Additionally, we empirically conduct an ablation comparing gradient consistency with another two
971 alternatives: (1) Softmax Confidence: For sample x_i , we compute the predicted class probabilities
972 $q_i = \text{softmax}(f_\theta(x_i))$. The confidence score is defined as $s_i = \max_j q_i^j$. Samples with lower
973 confidence are considered harder and are scheduled later in the curriculum. (2) Feature-space
974 Similarity (Prototype-based Selection): For each class j , we maintain a prototype vector w_j , typically
975

972 Table 14: Classification accuracy of different consistency metrics on CIFAR-100-C and DomainNet.
973

Methods	CIFAR-100-C	DomainNet
Gradient Consistency	60.11	37.35
Confidence	59.87	37.23
Feature	59.72	37.07

980 computed as the mean feature representation of samples in the batch. For sample x_i , we extract
981 its feature z_i and compute its distance to the nearest class prototype: $s_i = \min_j \|\phi_\theta(x_i) - w_j\|_2$.
982 Samples with larger distances are considered harder and scheduled later in the curriculum, while
983 samples closer to the prototype are scheduled earlier. Table 14 validates the effectiveness of gradient
984 consistency compared to confidence-based and feature-level selection strategies.
985

986 A.9 PERFORMANCE WITH OTHER SELECTION STRATEGIES

988 To validate the effectiveness of our curriculum-based scheduling, we compare it with random selection
989 and sequential (input-order) selection under the same test-time adaptation setup. Results are shown
990 in Table 15. Both random and sequential orders achieve similar performance, whereas our gradient-
991 consistency–driven curriculum consistently improves accuracy. This demonstrates that CUPLOT’s
992 gains are not due to arbitrary ordering but result from the proposed principled curriculum.
993

994 Table 15: Accuracy of different sequence strategies.
995

Methods	CIFAR-10-C	CIFAR-100-C	ImageNet-C
Sequential Selection	86.52	58.54	44.01
Random Selection	86.47	58.50	44.06
CUPLOT	87.35	60.11	55.21

1000 A.10 PLUG-AND-PLAY STUDY

1003 We conduct additional experiments integrating our gradient-consistency curriculum with two repre-
1004 sentative baselines: SHOT-IMLiang et al. (2020) and DEYOLee et al. (2024). In both cases, we replace
1005 their batch-level pseudo-labeling step with CUPLOT’s curriculum-based ordering while keeping
1006 all other components unchanged. The results in Table 16 support that the proposed curriculum
1007 is a general and complementary mechanism that enhances other TTA methods—not tied to our
1008 prototype-based instantiation.
1009

1010 Table 16: Accuracy improvements when integrating CUPLOT’s curriculum into SHOT-IMLiang et al.
1011 (2020) and DEYOLee et al. (2024) across corruption benchmarks.
1012

Methods	CIFAR-10-C	CIFAR-100-C	ImageNet-C
SHOT-IM	86.33	59.14	54.43
SHOT-IM+Ours	86.95	59.87	55.25
DeYO	86.14	59.08	50.43
DeYO+Ours	87.01	59.60	51.53

1019 A.11 FULL EXPERIMENTAL RESULTS

1022 Table 17, 18, 19, 20, 21, 22, 23, 24, 25, 26, and 27 present full results of each compared approach
1023 on datasets CIFAR-10-C, CIFAR-100-C, ImageNet-C, PACS, VLCS, OfficeHome, and
1024 DomainNet, respectively. Also, we present tSNE (Van der Maaten & Hinton, 2008) visualizations
1025 on the domain A of the benchmark dataset PACS for both the ERM baseline and our proposed
framework CUPLOT, as depicted in Figure 3 in Appendix A.11. Once adapted to the target domain,
1026

1026

1027

1028

1029

1030

1031

1032

1033

1034

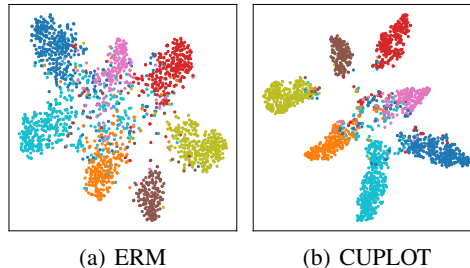
1035

1036

1037

1038

1039



(a) ERM (b) CUPLOT

Figure 3: tSNE visualization on PACS domain A.

Table 17: Full results on the CIFAR-10-C dataset.

Methods	shot	motion	snow	pixelate	gaussian	defocus	brightness	fog	zoom	frost	glass	impulse	coostraint	jpeg	elastic	Avg.
ERM	42.14	57.12	72.50	59.61	35.62	73.83	88.55	49.87	78.97	63.55	33.44	22.02	20.61	72.33	62.49	55.51
BN	84.05	87.30	85.51	89.40	82.69	90.99	92.33	83.31	92.63	87.99	75.17	72.84	89.86	85.87	82.33	85.48
TENT	84.38	87.53	85.76	89.62	83.12	91.11	92.44	83.87	92.77	88.10	75.83	73.46	90.53	86.12	82.52	85.81
PL	84.34	87.83	86.28	88.93	82.98	90.41	91.71	85.49	91.95	87.63	76.77	76.53	90.65	84.91	82.22	85.91
SHOT-IM	85.04	88.01	86.86	89.12	83.54	91.01	91.80	85.92	91.92	88.22	77.84	76.06	91.08	85.82	82.73	86.33
T3A	50.74	60.54	72.92	65.48	45.06	75.71	88.16	52.64	80.58	65.11	41.35	29.22	24.55	73.99	67.29	59.56
TAST	83.85	87.32	85.57	88.90	82.65	90.98	91.99	83.01	92.23	87.57	75.38	72.49	89.44	85.73	82.41	85.30
TAST-BN	84.87	87.94	86.10	89.98	83.62	91.27	92.45	84.21	92.76	88.30	76.50	74.28	89.83	86.35	83.14	86.11
TSD	85.02	88.30	86.69	89.94	83.96	91.40	92.60	85.12	92.94	88.61	76.92	75.05	91.10	86.79	83.18	86.51
PROGRAM	81.31	84.15	82.41	86.06	78.83	87.99	89.22	80.05	89.67	84.57	71.02	68.91	86.09	82.64	78.61	82.10
DEYO	84.58	87.78	87.01	88.68	83.48	90.35	91.71	85.94	92.15	87.48	76.66	76.38	91.32	86.05	82.54	86.14
CUPLOT	86.06	89.08	87.91	89.93	84.57	91.52	92.40	87.45	92.66	89.02	79.11	77.42	91.54	87.24	84.29	87.35

CUPLOT is capable of generating extracted features that are more clearly separated. These clearly indicate the significance of curriculum pseudo-labels in enhancing absorption of domain knowledge when the model is adapting.

A.12 THE USE OF LARGE LANGUAGE MODELS

We acknowledge the use of a large language model (LLM) as an assistive tool during the preparation of this manuscript. The LLM’s role was strictly limited to language-related refinements: specifically, it aided in grammar and spelling corrections, and helped enhance the logical coherence and readability of the prose. Additionally, the model provided support for generating certain segments of code. It is important to emphasize that the core conceptual framework, theoretical analyses, experimental design, and conclusions presented in this paper are the original work of the authors, with no involvement of the LLM in shaping these substantive research components.

Table 18: Full results on the CIFAR-100-C dataset.

Methods	shot	motion	snow	pixelate	gaussian	defocus	brightness	fog	zoom	frost	glass	impulse	coostraint	jpeg	elastic	Avg.
ERM	33.09	32.31	39.60	43.78	31.04	43.82	54.76	14.61	48.65	36.84	23.74	16.66	7.75	49.73	36.57	34.20
BN	55.63	58.14	54.38	64.50	55.53	63.92	65.13	43.27	67.74	58.67	48.19	42.50	56.30	62.56	53.77	56.68
TENT	56.33	58.70	54.62	64.77	55.92	64.41	65.61	44.25	68.03	59.09	48.86	43.07	57.35	62.89	54.30	57.21
PL	57.85	60.27	55.43	65.22	56.81	64.96	65.96	46.84	68.41	59.69	50.68	44.75	60.77	62.77	56.18	58.44
SHOT-IM	58.24	60.59	56.40	65.73	57.61	65.88	66.88	47.54	69.02	60.71	50.84	46.00	61.27	64.03	56.38	59.14
T3A	35.29	33.25	38.78	44.16	32.68	44.16	54.31	16.28	48.60	37.26	25.35	18.21	7.94	49.03	38.11	34.89
TAST	51.34	52.26	48.48	57.81	50.74	58.65	58.70	39.86	61.22	53.55	43.9	39.74	51.30	56.03	49.16	51.52
TAST-BN	50.42	52.32	47.83	57.69	49.93	57.70	58.07	39.33	60.71	52.31	43.48	38.95	51.03	55.67	48.38	50.92
TSD	57.74	59.81	55.89	65.54	57.20	65.65	66.62	46.21	68.91	60.14	49.90	44.51	60.26	63.57	55.40	58.49
PROGRAM	54.68	56.85	53.61	62.82	54.38	62.58	64.05	42.43	66.95	58.15	46.98	41.76	55.18	61.75	52.32	55.63
DEYO	58.06	61.13	56.18	65.30	57.13	65.75	66.42	48.41	68.64	59.77	51.26	45.87	62.13	63.52	56.61	59.08
CUPLOT	59.24	61.58	57.11	65.92	58.41	66.49	66.52	50.46	69.56	61.12	52.57	47.82	62.93	64.43	57.53	60.11

1080

1081

1082

Table 19: Full results on the ImageNet-C dataset.

1083

Methods	shot	motion	snow	pixelate	gaussian	defocus	brightness	fog	zoom	frost	glass	impulse	coostraint	jpeg	elastic	Avg.
ERM	46.10	36.70	40.66	61.72	43.90	27.58	69.36	31.10	30.24	41.76	21.58	44.12	4.62	59.66	41.62	40.05
BN	-	-	-	-	-	-	-	-	-	-	-	-	-	-	-	-
TENT	-	-	-	-	-	-	-	-	-	-	-	-	-	-	-	-
PL	53.78	50.18	53.52	69.10	52.64	42.52	73.08	47.72	39.76	50.06	40.66	51.74	3.68	66.66	54.80	49.99
SHOT-IM	55.74	53.60	55.40	69.76	54.00	45.00	73.30	51.66	48.54	53.72	48.18	54.00	27.24	67.82	58.54	54.43
T3A	45.94	36.58	40.72	61.80	43.84	27.34	69.36	28.00	30.22	41.50	21.12	44.04	3.26	59.60	41.70	39.67
TAST	38.90	31.32	36.10	53.44	37.04	23.46	61.32	27.90	26.62	36.44	17.80	37.18	3.90	50.56	38.06	34.67
TAST-BN	-	-	-	-	-	-	-	-	-	-	-	-	-	-	-	-
TSD	55.02	52.26	24.90	69.74	53.64	41.80	73.30	9.30	30.00	28.86	44.42	54.00	0.52	67.66	55.26	44.05
PROGRAM	46.58	30.14	26.04	62.60	43.36	32.40	67.42	3.94	34.72	16.06	3.18	43.64	1.18	60.40	45.02	34.45
DEYO	54.06	50.44	52.80	69.14	52.50	42.12	73.42	45.80	42.36	52.26	42.36	52.50	4.62	67.12	55.02	50.43
CUPLOT	56.10	54.40	56.48	70.34	54.02	46.44	73.56	52.78	50.02	54.76	49.38	54.34	28.12	68.08	59.32	55.21

1091

1092

1093

1094

1095

1096

1097

Table 20: Full results on the PACS dataset with ResNet-18.

Methods	A	C	P	S	Avg.
ERM	78.92 ± 1.59	76.42 ± 3.24	94.79 ± 0.63	70.20 ± 1.40	80.08
BN	82.36 ± 0.37	81.41 ± 0.79	95.87 ± 0.10	72.42 ± 0.77	83.02
TENT	82.55 ± 0.37	81.60 ± 0.74	96.03 ± 0.15	72.92 ± 0.56	83.28
PL	85.63 ± 0.82	84.47 ± 0.45	95.89 ± 0.54	77.30 ± 1.91	85.82
SHOT-IM	85.19 ± 1.02	81.25 ± 1.00	95.91 ± 1.02	68.45 ± 1.64	82.70
T3A	80.71 ± 1.48	79.29 ± 2.42	95.93 ± 0.52	73.09 ± 1.13	82.26
TAST	84.31 ± 0.52	82.95 ± 0.64	96.75 ± 0.21	74.40 ± 0.40	84.60
TAST-BN	84.80 ± 1.12	83.15 ± 0.62	96.63 ± 0.46	76.96 ± 0.99	85.39
TSD	87.92 ± 0.62	86.79 ± 0.18	96.65 ± 0.52	78.54 ± 2.65	87.48
PROGRAM	84.39 ± 1.37	79.25 ± 1.67	93.83 ± 4.21	72.54 ± 0.85	82.50
DEYO	86.31 ± 1.02	83.89 ± 0.80	96.11 ± 0.49	80.21 ± 0.13	86.63
CUPLOT	88.67 ± 0.81	87.74 ± 0.58	96.61 ± 0.59	78.47 ± 3.66	87.87

1110

1111

1112

1113

1114

1115

1116

1117

Table 21: Full results on the PACS dataset with ResNet-50.

Methods	A	C	P	S	Avg.
ERM	85.24 ± 1.79	79.65 ± 2.05	96.29 ± 0.68	80.71 ± 2.21	85.47
BN	86.51 ± 1.21	83.92 ± 1.96	96.55 ± 0.39	77.37 ± 0.86	86.09
TENT	86.82 ± 1.23	84.27 ± 1.89	96.61 ± 0.44	78.60 ± 0.88	86.58
PL	87.44 ± 1.53	82.51 ± 4.43	94.79 ± 2.13	79.77 ± 2.39	86.13
SHOT-IM	86.34 ± 0.54	82.75 ± 1.69	94.75 ± 0.30	77.55 ± 1.71	85.35
T3A	85.48 ± 2.19	81.08 ± 1.13	96.79 ± 0.28	80.68 ± 2.22	86.01
TAST	87.51 ± 0.94	84.09 ± 1.80	96.89 ± 0.74	77.75 ± 0.96	86.56
TAST-BN	89.18 ± 1.28	86.04 ± 1.38	97.11 ± 0.81	84.57 ± 0.39	89.23
TSD	90.97 ± 0.67	90.03 ± 0.99	97.42 ± 0.37	85.71 ± 0.13	91.03
PROGRAM	87.18 ± 1.38	84.26 ± 1.80	96.65 ± 0.31	77.65 ± 0.70	86.44
DEYO	88.72 ± 0.58	85.27 ± 1.61	96.79 ± 0.33	82.56 ± 0.99	88.34
CUPLOT	91.33 ± 1.15	90.00 ± 1.62	97.60 ± 0.57	85.51 ± 0.65	91.11

1130

1131

1132

1133

1134

1135

1136

Table 22: Full results on the VLCS dataset with ResNet-18.

1137

1138

1139

1140

1141

1142

1143

1144

1145

1146

1147

1148

1149

1150

1151

1152

1153

1154

Table 23: Full results on the VLCS dataset with ResNet-50.

1155

1156

1157

1158

1159

1160

1161

1162

1163

1164

1165

1166

1167

1168

1169

1170

1171

1172

Table 24: Full results on the OfficeHome dataset with ResNet-18.

1173

1174

1175

1176

1177

1178

1179

1180

1181

1182

1183

1184

1185

1186

1187

1188

Methods	C	L	S	V	Avg.
ERM	96.42 \pm 1.37	63.79 \pm 1.16	70.49 \pm 1.41	70.21 \pm 2.53	75.23
BN	82.64 \pm 2.50	59.22 \pm 0.90	62.91 \pm 2.10	70.19 \pm 1.34	68.74
TENT	83.23 \pm 2.41	59.61 \pm 0.99	63.47 \pm 2.18	70.70 \pm 1.06	69.25
PL	91.92 \pm 1.31	62.41 \pm 1.16	69.61 \pm 1.20	74.44 \pm 1.85	74.60
SHOT-IM	89.47 \pm 3.48	58.85 \pm 1.24	64.16 \pm 2.85	71.49 \pm 0.69	70.99
T3A	99.32 \pm 0.18	63.89 \pm 1.66	69.99 \pm 1.90	70.51 \pm 2.77	75.93
TAST	94.65 \pm 1.45	55.58 \pm 2.32	62.78 \pm 3.27	70.50 \pm 1.58	70.88
TAST-BN	97.45 \pm 0.76	62.58 \pm 5.78	65.65 \pm 0.79	74.38 \pm 2.34	75.02
TSD	94.35 \pm 3.15	64.82 \pm 1.03	66.94 \pm 1.48	73.11 \pm 2.66	74.81
PROGRAM	95.87 \pm 1.45	59.88 \pm 0.61	64.08 \pm 4.68	69.58 \pm 0.60	72.35
DEYO	93.47 \pm 2.93	60.42 \pm 6.09	68.18 \pm 2.60	74.13 \pm 1.62	74.05
CUPLOT	99.41 \pm 0.15	65.61 \pm 0.50	71.25 \pm 2.23	71.61 \pm 1.40	76.97

Methods	A	C	P	R	Avg.
ERM	55.51 \pm 0.41	48.93 \pm 0.36	71.58 \pm 0.52	73.61 \pm 0.46	62.41
BN	54.79 \pm 0.32	49.41 \pm 0.88	70.99 \pm 0.83	73.24 \pm 0.46	62.11
TENT	54.95 \pm 0.37	49.66 \pm 0.79	71.27 \pm 0.89	73.33 \pm 0.48	62.30
PL	55.16 \pm 0.32	50.38 \pm 0.65	71.02 \pm 1.32	73.58 \pm 0.10	62.54
SHOT-IM	56.25 \pm 0.64	51.59 \pm 0.54	72.83 \pm 0.06	73.81 \pm 0.47	63.62
T3A	56.04 \pm 0.75	50.92 \pm 0.46	73.67 \pm 0.41	74.70 \pm 0.76	63.83
TAST	55.33 \pm 0.80	50.94 \pm 1.25	73.96 \pm 0.90	73.90 \pm 1.04	63.53
TAST-BN	54.74 \pm 0.38	50.36 \pm 0.78	72.35 \pm 0.78	71.85 \pm 0.23	62.33
TSD	56.90 \pm 0.48	50.03 \pm 1.30	72.17 \pm 0.97	73.38 \pm 0.25	63.12
PROGRAM	55.62 \pm 0.61	50.09 \pm 1.83	72.07 \pm 0.08	73.74 \pm 0.57	62.88
DEYO	56.38 \pm 0.25	50.36 \pm 0.70	71.86 \pm 1.08	73.60 \pm 0.30	63.05
CUPLOT	57.31 \pm 0.57	52.11 \pm 0.80	73.96 \pm 0.45	74.82 \pm 0.45	64.55

1188

1189

1190

Table 25: Full results on the OfficeHome dataset with ResNet-50.

1191

Methods	A	C	P	R	Avg.
ERM	62.93 \pm 0.36	53.35 \pm 0.82	76.27 \pm 0.09	78.21 \pm 0.42	67.69
BN	62.67 \pm 0.36	53.46 \pm 0.45	75.08 \pm 0.66	77.52 \pm 0.80	67.18
TENT	62.96 \pm 0.30	54.26 \pm 0.39	75.18 \pm 0.55	77.53 \pm 0.72	67.48
PL	63.73 \pm 0.41	55.21 \pm 0.60	73.64 \pm 0.98	77.85 \pm 0.69	67.61
SHOT-IM	63.59 \pm 1.12	54.28 \pm 0.16	75.96 \pm 0.41	78.10 \pm 0.59	67.98
T3A	63.25 \pm 0.22	54.95 \pm 0.85	77.79 \pm 0.21	79.04 \pm 0.12	68.76
TAST	63.62 \pm 0.27	55.46 \pm 0.81	77.51 \pm 0.63	78.21 \pm 0.59	68.70
TAST-BN	63.78 \pm 0.34	55.76 \pm 0.73	76.84 \pm 0.49	78.01 \pm 0.28	68.60
TSD	64.73 \pm 0.41	57.15 \pm 0.55	76.78 \pm 0.54	77.78 \pm 0.70	69.11
PROGRAM	63.55 \pm 0.79	54.27 \pm 0.29	76.27 \pm 1.01	77.85 \pm 0.77	67.99
DEYO	63.96 \pm 0.27	55.22 \pm 0.91	75.96 \pm 0.42	77.87 \pm 0.85	68.25
CUPLOT	66.64 \pm 0.69	57.87 \pm 0.55	77.62 \pm 0.32	79.05 \pm 0.15	70.30

1204

1205

1206

1207

1208

1209

1210

1211

Table 26: Full results on the DomainNet dataset with ResNet-18.

1212

Methods	clipart	infograph	painting	quickdraw	real	sketch	Avg.
ERM	50.42 \pm 0.13	15.32 \pm 0.15	41.83 \pm 0.09	11.46 \pm 0.43	51.74 \pm 0.34	43.64 \pm 0.21	35.74
BN	50.75 \pm 0.11	11.26 \pm 0.21	40.71 \pm 0.18	11.12 \pm 0.12	51.86 \pm 0.30	43.70 \pm 0.23	34.90
TENT	51.16 \pm 0.12	12.47 \pm 0.23	41.84 \pm 0.25	10.65 \pm 0.33	51.28 \pm 0.20	44.76 \pm 0.17	35.36
PL	50.88 \pm 0.06	13.16 \pm 0.37	41.19 \pm 0.15	10.69 \pm 0.57	51.72 \pm 0.42	44.02 \pm 0.26	35.28
SHOT-IM	50.90 \pm 0.13	12.76 \pm 0.39	41.36 \pm 0.18	13.58 \pm 0.11	52.37 \pm 0.30	44.38 \pm 0.23	35.89
T3A	50.36 \pm 0.29	15.14 \pm 0.15	40.26 \pm 0.05	16.22 \pm 0.19	53.02 \pm 0.13	42.74 \pm 0.26	36.29
TAST	50.43 \pm 0.27	10.67 \pm 0.05	40.69 \pm 0.09	14.22 \pm 0.19	53.69 \pm 0.33	42.49 \pm 0.26	35.37
TAST-BN	50.12 \pm 0.31	11.32 \pm 0.13	40.82 \pm 0.19	14.11 \pm 0.29	52.11 \pm 0.21	42.19 \pm 0.31	35.11
TSD	50.75 \pm 0.13	11.71 \pm 0.13	42.35 \pm 1.17	11.96 \pm 0.67	52.03 \pm 0.33	44.20 \pm 0.21	35.50
PROGRAM	50.95 \pm 0.08	13.09 \pm 0.33	41.67 \pm 0.15	13.28 \pm 0.24	52.35 \pm 0.34	44.27 \pm 0.25	35.94
DEYO	50.85 \pm 0.05	13.23 \pm 0.25	41.20 \pm 0.18	10.99 \pm 0.17	51.89 \pm 0.33	43.98 \pm 0.27	35.36
CUPLOT	51.77 \pm 0.11	14.95 \pm 0.06	42.29 \pm 0.11	15.89 \pm 0.27	54.48 \pm 0.28	44.72 \pm 0.24	37.35

1223

1224

1225

1226

1227

1228

Table 27: Full results on the DomainNet dataset with ResNet-50.

1229

Methods	clipart	infograph	painting	quickdraw	real	sketch	Avg.
ERM	61.14 \pm 0.23	20.89 \pm 0.23	49.74 \pm 0.29	13.68 \pm 0.29	62.08 \pm 0.20	52.20 \pm 0.41	43.29
BN	60.58 \pm 0.23	15.19 \pm 0.12	48.66 \pm 0.12	11.95 \pm 0.24	61.18 \pm 0.26	51.66 \pm 0.15	41.54
TENT	61.71 \pm 0.24	17.36 \pm 0.09	50.33 \pm 0.13	10.26 \pm 0.77	61.58 \pm 0.18	53.27 \pm 0.08	42.42
PL	61.04 \pm 0.22	17.62 \pm 0.43	49.93 \pm 0.06	11.75 \pm 0.47	61.37 \pm 0.17	52.59 \pm 0.19	42.38
SHOT-IM	61.40 \pm 0.39	17.51 \pm 0.09	49.82 \pm 0.13	16.54 \pm 0.53	62.65 \pm 0.18	52.81 \pm 0.21	43.46
T3A	61.13 \pm 0.34	21.01 \pm 0.18	48.82 \pm 0.11	18.67 \pm 0.49	63.32 \pm 0.15	51.69 \pm 0.33	44.11
TAST	60.77 \pm 0.42	14.95 \pm 0.20	48.96 \pm 0.14	15.16 \pm 0.27	62.85 \pm 0.36	51.56 \pm 0.18	42.38
TAST-BN	60.89 \pm 0.29	15.31 \pm 0.25	48.99 \pm 0.09	14.92 \pm 0.23	62.98 \pm 0.28	51.83 \pm 0.19	42.49
TSD	60.80 \pm 0.29	15.52 \pm 0.11	49.42 \pm 0.08	13.88 \pm 0.24	61.70 \pm 0.19	52.28 \pm 0.18	42.27
PROGRAM	61.15 \pm 0.26	18.05 \pm 0.08	49.99 \pm 0.28	15.48 \pm 0.40	62.23 \pm 0.15	53.22 \pm 0.21	43.35
DEYO	61.03 \pm 0.21	18.05 \pm 0.32	49.89 \pm 0.09	12.00 \pm 0.25	61.33 \pm 0.13	52.51 \pm 0.21	42.47
CUPLOT	62.34 \pm 0.19	20.76 \pm 0.18	50.48 \pm 0.01	18.60 \pm 0.52	64.57 \pm 0.19	53.15 \pm 0.33	44.98

1239

1240

1241